Integrative Biology

Accepted Manuscript

This is an *Accepted Manuscript*, which has been through the Royal Society of Chemistry peer review process and has been accepted for publication.

Accepted Manuscripts are published online shortly after acceptance, before technical editing, formatting and proof reading. Using this free service, authors can make their results available to the community, in citable form, before we publish the edited article. We will replace this *Accepted Manuscript* with the edited and formatted *Advance Article* as soon as it is available.

You can find more information about *Accepted Manuscripts* in the Information for Authors.

Please note that technical editing may introduce minor changes to the text and/or graphics, which may alter content. The journal's standard Terms & Conditions and the Ethical guidelines still apply. In no event shall the Royal Society of Chemistry be held responsible for any errors or omissions in this *Accepted Manuscript* or any consequences arising from the use of any information it contains.

ROYAL SOCIETY OF CHEMISTRY

www.rsc.org/ibiology

Graphical abstract

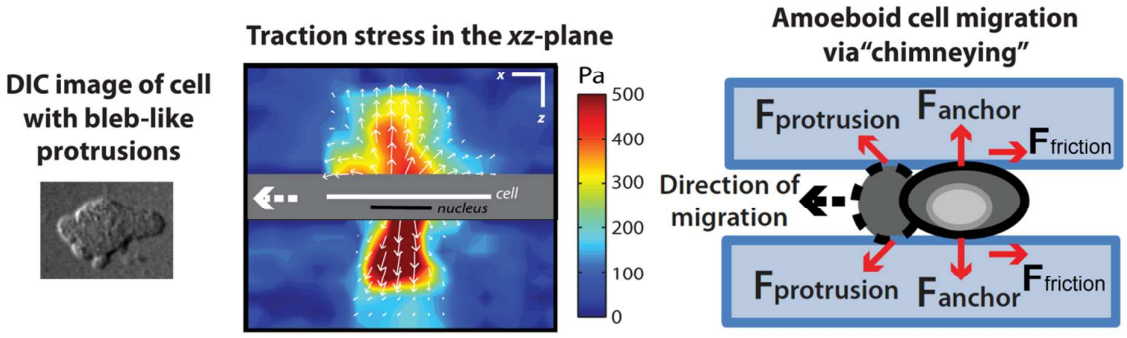

Neutrophil-like cells, confined between two non-fibronectin-coated gels, form blebs and generate expansive forces against opposing surfaces during amoeboid cell "chimneying".

Integrative Biology Accepted Manuscript

Insight box

A leukocyte can translocate across a surface by either a mesenchymal or amoeboid mechanism. While integrin-dependent mesenchymal migration is well understood, little is known about the nature of the traction forces required for amoeboid migration in the absence of cell-matrix adhesions. Here, we have combined 3-dimensional traction force microscopy with a confinement assay, where neutrophil-like cells are confined between two pieces of polyacrylamide gels. In the absence of cell-matrix adhesions, confined cells migrate by "chimneying", that is, generate traction by applying forces against opposing surfaces. Chimneying speed was fastest at an intermediate spacing between the two gels. A computational model explains that chimneying speed depends on both the magnitude of the intracellular pressure and the location where blebs form as determined by the membrane-cortex adhesion strength.

Integrative Biology Accepted Manuscript

Traction stress analysis and modeling reveal amoeboid migration in confined spaces is accompanied by expansive forces and requires the structural integrity of the membrane-cortex interactions.

Ai Kia Yip,[§] Keng-Hwee Chiam,[‡§]* and Paul Matsudaira[‡¶]*

[§]A*STAR Bioinformatics Institute, Singapore

[‡]MechanoBiology Institute, National University of Singapore, Singapore

[¶]Department of Biological Sciences, NUS Centre for BioImaging Sciences, National University of Singapore, Singapore

*Corresponding authors:

Keng-Hwee Chiam

A*STAR Bioinformatics Institute, 30 Biopolis Street, #07-01 Matrix, Singapore 138671

Phone: +65 6478-8264

E-mail: chiamkh@bii.a-star.edu.sg

Paul Matsudaira

Department of Biological Science, National University of Singapore, 14 Science Drive 4, Singapore 117543

Phone: +65 6516-2692

E-mail: dbsmpt@nus.edu.sg

Integrative Biology Accepted Manuscript

Abstract

Leukocytes and tumor cells migrate via rapid shape changes in an amoeboid-like manner, distinct from mesenchymal cells such as fibroblasts. However, the mechanisms of how rapid shape changes are formed and how they lead to migration in the amoeboid mode are still unclear. In this study, we confined differentiated human promyelocytic leukemia cells between opposing surfaces of two pieces of polyacrylamide gels and characterized the mechanics of fibronectin-dependent mesenchymal versus fibronectin-independent amoeboid migration. On fibronectin-coated gels, the cells form lamellipodia and migrate mesenchymally. Whereas in the absence of cell-substrate adhesions through fibronectin, the same cells migrate by producing blebs and "chimneying" between the gel sheets. To identify the orientation and to quantify the magnitude of the traction forces, we found by traction force microscopy that expanding blebs push into the gels and generate anchoring stresses whose magnitude increases with decreasing gap size while the resulting migration speed is highest at an intermediate gap size. To understand why there exists such an optimal gap size for migration, we developed a computational model and showed that chimneying speed depends on both the magnitude of intracellular pressure as well as the distribution of blebs around the cell periphery. The model also predicts that the optimal gap size increases with weakening cell membrane to actin cortex adhesion strength. We verified this prediction experimentally, by weakening the membrane-cortex adhesion strength with the ezrin inhibitor, baicalein. Thus, the chimneying mode of amoeboid migration requires a balance between intracellular pressure and membrane-cortex adhesion strength.

Integrative Biology Accepted Manuscript

Introduction

Cell migration is a crucial process during embryonic development (1-3), wound closure (4,5), and as part of the body's immune response (6,7). During cancer cell metastasis, cancer cells also migrate into and out of the lymphatic and blood vessels to cause secondary growth (8,9). The study of cell migration mechanisms is therefore important in developing therapies to restore normal functioning of the organisms, or to stop cancer cells from spreading to secondary sites.

Studies of cell migration originated first from observations of the unicellular protozoa, amoeba. The amoeba migrates via a sterotypic manner by extending its pseudopodia forward and coordinating cytoplasmic streaming (10-16). Recent studies have also shown that cells from multicellular organisms, such as leukocytes, zebrafish primordial germ cells and selected tumor cells, also exhibit amoeboid-like movements (9,17-21). These cells form round bleb-like protrusions and change their shapes rapidly, similar to the amoeba (9,17,21). The rapid shape changes allow the cells to squeeze through pre-existing gaps in the three-dimensional (3D) matrix without having to degrade the extracellular matrix (ECM) (9,18) or adhere to the ECM (19,22).

However, not all cells move in an amoeboid-like manner. A second mode of cell migration, termed mesenchymal cell migration, is exhibited by mesenchymal cells such as fibroblasts, keratocytes and epithelial cells crawling on two-dimensional (2D) surfaces (9,23-26). During cell migration, mesenchymal cells form finger-like (filopodia) (27) or sheet-like (lamellipodia) protrusions rich with filamentous actin (F-actin) (23,28,29). These protrusions come into contact with the surrounding ECM and adhere to the ECM proteins (e.g. fibronectin and collagen) through integrin-mediated focal adhesion complexes (26,28) (Fig. 1*A*). The focal adhesion complexes disassemble at the rear of the cell to allow the cell to detach at trailing edge as the myosin II which binds to the actin filaments (actomyosin) contract (9). In this way, the cell exerts contractile traction forces on the underlying substrates as the cell body moves forward (30-34).

Although much has been known about the mechanism employed by mesenchymal cells during cell migration, the amoeboid cell migration mechanism remains a mystery. How do amoeboid cells translate rapid shape changes to cell migration? How can the cells exert forces and translocate if the cells do not adhere to the surrounding matrix? Malawista *et. al* explained that cells can continue to migrate, in the absence of cell-matrix adhesions, when confined between two glass coverslips, via a mechanism known as "chimneying" (22). During chimneying, Charras and Paluch proposed that the cell exerts forces perpendicularly to the surfaces such that it can squeeze itself forward by blebbing (17) (Fig. 1*B*). However, these forces have not been directly shown or quantified. In addition, some cancer cells that are treated with drugs which inhibit mesenchymal cell migration have been shown to be able to switch to the amoeboid mode of migration (mesenchymal to amoeboid transition) (18,20). Lammermann *et. al* also observed that leukocytes are capable of migration via both integrin-dependent and -independent mechanism (19). An understanding of the requirements of both the amoeboid and mesenchymal cell migration mechanism can therefore be crucial in designing treatments to prevent cancer cell metastasis or to understand leukocyte recruitment during inflammation.

In this report, we proposed a system to compare the mechanics of amoeboid cell migration by chimneying with the mechanics of mesenchymal cell migration by crawling as cells migrate between closely spaced layers of polyacrylamide gels (Fig, 2*A-B*). In our

Integrative Biology Accepted Manuscript

experiments, a human promyelocytic leukemia (HL60) cell line was differentiated to model neutrophil-like cells, commonly used to study neutrophil chemotaxis. Studies have shown that neutrophils can adhere to fibronectin-coated substrates and migrate towards a chemoattractant (e.g. Formyl-Methionyl-Leucyl-Phenylalanine) by forming lamellipodia (35). Here, we showed that the neutrophil-like differentiated human promyelocytic leukemia (dHL60) cells confined between two pieces of polyacrylamide gels, can exhibit two different migration modalities. When the gels are coated with fibronectin, most of the cells form lamellipodia and migrate mesenchymally on 2D surfaces and in between the confining gels. When the gels are not coated with fibronectin, the cells formed blebs but could not translocate until they are confined between two pieces of gels where they can push against the confining gels and migrate in an amoeboid chimneying manner. From the displacement of beads embedded in the gel, we were able to calculate the three-dimensional (3D) gel traction stresses exerted by the cell.

The ability of the neutrophil-like dHL60 cells to exhibit either the mesenchymal or the amoeboid mode of motility by simply changing the ECM adhesivity allowed us to explore how cells migrating in the two modes of migration respond differently to mechanical changes of the ECM. By varying the gel rigidity and spacing of the gap between the gels, our results showed that amoeboid chimneying speed is biphasic with respect to gap distance but independent on gel rigidity. We have also developed a computational model to explain the relationship between the gel gap spacing and the symmetry of blebbing. Our model explains how the balance between two forces, intracellular pressure and membrane-cortex adhesion strength, determines the speed of migration. To test the model, we perturbed the membrane-cortex with the ezrin inhibitor, baicalein, and observed the predicted shift by the biphasic curve to an increased gap size. Although our experimental results was obtained based on a neutrophil-like cell line, the model mechanisms proposed could provide generic insights regarding amoeboid cell migration in confined environments.

Results

Confined vs unconfined cell migration on polyacrylamide substrates

To characterize cell migration between closely spaced substrates, we first examined unconfined cell migration on a 2D sheet of polyacrylamide gel. When the gels were coated with a hydrophilic, non-ionic surfactant, 0.1% Pluronic F127 (Pluronic-coated gel), the dHL60 cells were unable to adhere to the surfaces. The non-adherent cells in suspension changed shape with rapid blebbing but there was no translocation of the cell. In contrast, when cells were seeded on a single piece of fibronectin-coated (100 μg/ml) gel (unconfined conditions), the dHL60 cells adhered to the gel surface and exhibited mesenchymal-type migration with the lamellipodia-like protrusions at their leading edge (Fig. 2*C solid boxes*). We also observed some non-adherent cells in suspension and they also formed bleb-like protrusions (Fig. 2*C dashed boxes*).

The dHL60 cells can also be confined between two pieces of gels when the distance between a top and bottom gel (gap spacing) is smaller than the cell diameter (2-8 μm, confined conditions). We quantified the type of motility as a function of substrate coating on polyacrylamide gels with Young's moduli of 1.25 to 16.6 kPa. When the cells were confined between two pieces of Pluronic-coated gels (16.6 kPa) separated by a 2-8 μm gap, where the dHL60 cells were in contact with but not adherent to opposing Pluronic-coated gels, we found that 59.1% of the cells migrated in an amoeboid-like manner by producing bleb-like

Integrative Biology Accepted Manuscript

protrusions (Fig. 2*D-E*). 5.5% of the cell population formed sheet-like protrusion resembling lamellipodia. The remaining 35.4% of cell population switched between bleb- and lamellipodia-type motility during imaging. On the other hand, lamellipodia-based, mesenchymal migration was found to be the dominant mode (60.3%) of cell migration when cells are confined between fibronectin-coated gels (Fig. 2*F-G*). Cells which formed blebs, or switched between bleb- and lamellipodia-type motility during imaging constituted only 0.8% or 38.9% of the cell population respectively (Fig. 2*H*). Similar results were also observed on the softer gels (1.25 kPa and 6.19 kPa, Fig. 2*H*).

To confirm that the protrusions of cells confined between Pluronic-coated gels were blebs and not lamellipodia or filopodia, we visualized the F-actin localization within the dHL60 cells after transfection with Lifeact-GFP. When cells that were confined between Pluronic-coated gels formed the bleb-like protrusions, the blister-like protrusion was seen to be initially devoid of F-actin (Fig. 2*I arrow*). Subsequently, F-actin reappeared underneath the cell membrane (Fig. 2*J arrow*, Movie S1) (21,36,37) before the formation of another new bleb (Fig. 2*J arrowhead*). This is similar to previous reports that the cell membrane initially separates from the actin cortex during bleb formation and reforms under the cell membrane during bleb retraction (17,21,36,38). Conversely, F-actin localization in cells confined between fibronectin-coated gels, was seen to be always enriched at the cell front where the sheet-like protrusions formed (Fig. 2*K arrow,* Movie S2), in agreement with previous observations of the lamellipodia (9,25,36,37).

We next investigated the dependence of migration speed of confined cells on the stiffness of the substrate. Surprisingly, the dHL60 cells confined between Pluronic-coated gels migrated at a constant speed (3.53-3.71 μm/min), regardless of the gel rigidity (1.25-16.6 kPa; Fig. 3*A left*). This showed that chimneying speed is independent of gel rigidity. In contrast, the cells that were confined between fibronectin-coated gels and migrated in a mesenchymal manner showed a weak but detectable biphasic dependence on gel rigidity with the fastest speed occurring when cells were confined between 6.19 kPa gels (3.35 ± 0.17 μm/min, mean ± standard error; Fig. 3*A middle*). This trend was similarly observed for cells on fibronectin coated substrates in unconfined conditions (Fig. 3*A right*) and agrees well with previous studies which have reported that mesenchymal cells display a biphasic relationship between cell speed and substrate rigidity (39-41). However, cells confined between fibronectin-coated gels migrated with a slower speed as compared to cells that were unconfined, possibly because they are in contact with two adhesive gel surfaces which slowed migration speed.

We also observed that the dHL60 cells which were confined between Pluronic-coated gels moved slightly faster but with lesser persistence in their direction of movement as compared to cells confined between fibronectin-coated gels of the same rigidity (16.6 kPa, Fig. 3*B* and *C*). To quantify the persistence of cell movement, we have calculated the mean square displacement (MSD). A slope of $\beta = 0.93$ was obtained for cells confined between the Pluronic-coated gels, which indicates random diffusive movement (Fig. 3*D solid line*). In comparison, dHL60 cells that were confined between the fibronectin-coated gels moved with more persistence as revealed by a slope of $\beta = 1.74$, which indicates directed motion (Fig. 3*D dashed line*).

Cells migrating in the amoeboid mode generate normal stresses to anchor to the substrate and shear stresses to migrate at bleb protrusions

Integrative Biology Accepted Manuscript

To explain how movement occurs in the absence of fibronectin-mediated cell-matrix adhesion, we postulated that dHL60 cells migrated by chimneying (17), generating traction force by pushing against the confining gels. To confirm this hypothesis, we mapped the stresses exerted by the cells on the gels by three-dimensional (3D) traction force microscopy. We found that dHL60 cells confined between Pluronic-coated gels exerted mainly normal stresses (along the *z*-axis perpendicular to the plane of the gels) into both gel surfaces (Fig. 4*C*-*D*, $\vec{F}_{\text{anchor}}$). The magnitudes of these normal stresses (approximately 200-400 Pa) correspond to measurements of the intracellular pressure reported elsewhere (43), suggesting that the stresses originate from the cell's intracellular pressure which pushes against the confining gels. We also noticed that the chimneying cell exerts expansive shear stresses along the *xy*-plane pointing away from the cell body at both the front and the rear end of the cell (Fig. 4*B*). We postulate that these stresses arise due to the bleb protrusion at the cell front ($\vec{F}_{\text{protrusion}}$) and the friction between the cell and gel at the cell rear as actomyosin contraction drives the cell forward ($\vec{F}_{\text{friction}}$). The combination of the normal and shear stresses helped to anchor the cells between the gels in the absence of cell-matrix adhesion, and create the friction necessary to allow the cell to migrate.

To fully characterize the chimneying behaviour of the amoeboid cell, we performed a time-lapse traction force measurement during amoeboid cell migration. We observed that when a bleb is produced, very weak stresses are initially seen at the bleb region. Instead, the cell exerted anchoring stresses which were directed perpendicularly to the gels (Fig. 5*A*-*C*) at regions away from the bleb. However, as the cell cortex reformed underneath the bleb during bleb retraction, the cell squeezed itself forward and gradually anchored at the region where the bleb used to be located. This was seen as new anchoring stresses appeared at the region where the bleb was previously located (Fig. 5*D*-*F*). The anchoring stresses subsequently moved fully into the region at a later time frame (Fig. 5*G*-*I*). We also note that shear stresses directed opposite to the direction of cell migration appeared at the rear of the cells and this could be due to friction which opposes motion as the cell push off the gel surface (Fig. 5*D*,*G*).

To verify our hypothesis that amoeboid cells chimney by progressively exerting forces at the regions where the blebs were formed, we evaluated the average stress exerted, on the surface of the top and bottom gel, at the region where the bleb was initially observed at t = 0s (dotted line). We compared this stress with the average stress exerted elsewhere in the cell body as time progressed (Figure 5J). Indeed we found that as time progressed, the average stress in the region where the bleb was initially located increased as the cell migrates into the region, thereby resulting in a decrease in average stress at where other parts of the cell body was originally located.

We also hypothesized that as the gap size between the top and bottom gels increased, the chimneying cell will lose contact with the confining gels and the anchoring normal stresses will decrease. Indeed, the magnitude of the net normal stresses over the whole cell at the z-plane immediately next to the cell ($F_{z,net}$ as defined in the methods), was found to decrease significantly from 9.28 kPa to 3.06 kPa as the gap size increased from 2 μm to 8 μm (Fig. 6*A solid circles*, *C*, *E*, *G*). Similarly, with the increasing gap size, we observed that the average stress magnitude, $\langle F_{x,y,z} \rangle$, across the cell area at the top gel surface was decreased from 302 Pa to 124 Pa (Fig. 6*B solid circles*, *C*, *E*, and *G*). These results indicate that the cell pushes on the confining gels with a smaller force as gap size increased.

Integrative Biology Accepted Manuscript

Unlike the expansive and outwardly divergent traction stresses exerted by the chimneying cells, traction stresses exerted during mesenchymal migration were contractile and inwardly convergent in nature. These cells exerted large opposing shearing stresses on the top gels at the cell front and rear (Fig. 4*G-H*, $\vec{F}_{protrusion\ //}$ and $\vec{F}_{retraction\ //}$ respectively). Additional stresses along the *z*-axis are directed into the gel as cells protruded and pushed into the gels at their cell front (Fig. 4*H*, $\vec{F}_{protrusion\ \perp}$). On the other hand, the rear of the cells exerted stresses along the *z*-axis that were directed out of the gel (Fig. 4*H*, $\vec{F}_{retraction\ \perp}$) as cells detached and pulled from the gel at the rear. This "push-pull" dynamics of the cell have similarly been reported in other studies involving fibroblasts, a mesenchymal cell type (44). As the normal stresses due to protrusion and retraction of the dHL60 cells that migrate mesenchymally were in opposing directions, $F_{z,net}$ was maintained at a low value (compared with $F_{z,net}$ for chimneying cells) between 2.44 kPa to 2.90 kPa regardless of the gap size (Fig. 6*A open circles*). Although the average stress magnitude, $\langle F_{x,y,z} \rangle$, across the cell area at the top gel surface for cells that migrate mesenchymally decreased from 307 Pa to 215 Pa as gap size increased, the change was not statically significant, indicating that the cells adhered and remained in contact with the gels despite variations in the gap size (Fig. 6*B open circles*, *D*, *F* and *H*). However, we also noticed that the mesenchymal cells exert comparatively lower traction stresses on the bottom gel (Fig. 4*I-J*). We think that this is because we allowed the cells to adhere to the top gel first before inverting the top gel over another bottom gel, in our assembly of the confined environment, and thereby the cell adheres more strongly to the top gel as compared to the bottom gel. To verify this, we repeated the traction force measurements for a cell that was initially plated on the fibronectin-coated bottom gel and subsequently confined with a top gel. We showed that the overall traction stresses on the bottom gel was higher than that on the top gel for the cell first plated on a bottom gel, thereby verifying that the difference in the traction stresses was due to the initial plating location (Fig. S1).

Chimneying speed is maximal at an intermediate gap size

From the traction stress measurements at different gap spacings, we observed that the anchoring stress of the amoeboid cells decreased as they lose contact with the confining gels. This behavior indicates a dependence of cell speed on the anchoring traction stress. Therefore we measured cell speed as a function of gap spacing. Our results showed that amoeboid dHL60 cells confined between Pluronic-coated gels displayed a clear biphasic relationship between cell migration speed and gap size. The fastest speed occurred at an intermediate gap size of 6 μm (5.09 ± 0.36 μm/min, mean ± standard error) (Fig. 7*A solid squares*). To test the dependence on the formation and protrusion of blebs, we treated the cells with 50 μM (final concentration) of blebbistatin, a myosin II inhibitor which prevents bleb but not lamellipodia formation (45,46). After blebbistatin treatment, the cell speeds decreased (to approximately 0.5 μm/min) and were independent of gap size (Fig. 7*A solid circles*). However, when cells were confined in between fibronectin-coated gels, cell speeds were not significantly changed by either gap size or the addition of blebbistatin (1.80-2.04 μm/min) (Fig. 7*A open squares* and *open circles*). Thus, this biphasic relationship is exclusive to migration by chimneying, and is not observed for migration by lamellipodia formation.

To explain why amoeboid chimneying speed exhibits a biphasic relationship with gap size, we have quantified the number and the location where blebs were formed as the gap size decreased. The dHL60 cells confined between Pluronic-coated gels were found to produce more blebs when gap size decreased (Fig. 7*B solid squares*). The increased number of bleb

Integrative Biology Accepted Manuscript

protrusions was accompanied by a larger anchoring stress (Fig. 6*A solid circles*, *C*, *E*, *G*). However, we also observed that at extremely small gap sizes (2-4 μm), blebs were formed on opposing sides of the cell that potentially slowed migration (compare Movie S3 and S4). As a measure of protrusion asymmetry, we measured the angles formed between neighboring blebs and quantified the coefficient of variance (CV) as described in the methods. A large CV indicates protrusion asymmetry, with blebs generally formed on one side of the cell (polarized blebs). On the other hand, a CV value of 0 indicates symmetric protrusions whereby blebs are formed on opposing sides of the cell (non-polarized blebs). We found that the CV of angles between neighboring blebs decreased as the gap sizes decreased (Fig. 7*B open circles*). More non-polarized blebs formed on opposing sides of the cell reduces motility at very small gap sizes.

Computational modeling reveals that intracellular pressure and membrane-cortex adhesion strength determine optimum gap size

Finally, to provide an in-depth understanding of the mechanisms involved in amoeboid cell migration in a confined environment, we developed a computational model of a 2D cell (47,48, Fig. *S5* and Supplementary Information). The model of the cell, surrounded by an incompressible viscous fluid and confined between two channel walls of different spacing, is described by the 2D Stokes equation with no-slip boundary condition. The cell is comprised of an elastic cell membrane that is connected, through elastic membrane-cortex adhesion bonds, to a permeable elastic actin cortex. Detachment of the cell membrane from the actin cortex, by breaking the membrane-cortex adhesion bonds, resulted in bleb growth. Subsequently, actin monomers moved towards the detached cell membrane at a constant speed to reform the actin cortex underneath the cell membrane, and the blebs retract. Although the cell in the computational model does not adhere to the channel walls through a specific cell-substrate interaction (e.g. integrin-fibronectin adhesion bond), a no-slip boundary condition was imposed on the fluid in contact with the walls. In this way, the walls interact with the cell membrane hydrodynamically and provide the friction to resist relative motion at the channel walls.

Similar to experimental observations, the computational model revealed a biphasic relationship between the cell migration speed and the extent of cell confinement. The maximal cell speed predicted by the model occurred at an intermediate gap size (ratio of gap size to cell diameter (G/D) > 0.6 (Fig. 7*C*). The dHL60 cell diameter is experimentally measured to be approximately 9.21 ± 0.088 μm (mean ± standard error) (Fig. S3)). It was also observed that as the gap size decreased, intracellular pressure increased due to an increase in the extent of cell confinement (Fig. 7*D solid squares*). At higher intracellular pressures larger blebs form at the cell front and lead to faster chimneying speeds (Fig. 7*E* and *F*). The model also predicted that when intracellular pressure exceeded a critical threshold at very small gap sizes (G/D < 0.6), non-polarized blebs would be formed at both ends of the cell (Fig. 7*G*), hence lowering the CV of the angles between neighboring blebs (Fig. 7*D open circles*). As a result, cell speed decreased. These computational results agreed with our experimental observations of a biphasic relationship between amoeboid chimneying speed and the gap size.

In addition, the model predicted that the optimum gap size, where amoeboid chimneying speed is the fastest, could be increased by weakening the cell membrane to actin cortex adhesion strength (Fig. 7*H*). This membrane-cortex adhesion strength is mediated by

Integrative Biology Accepted Manuscript

proteins such as ezrin, radixin, and moesin (known collectively as the ERM proteins) (17,49,50). The model prediction was tested experimentally by inhibiting ezrin expression and phosphorylation with the inhibitor, baicalein (20 μM, final concentration) (51). We have verified with western blotting that the total ezrin expression levels in dHL60 cells decreased after 24 h of treatment with baicalein (inset in Fig. 7*I*). When dHL60 cells were treated with baicalein for 24 h and subsequently confined between Pluronic-coated gels, the optimum gap size where chimneying speed peaked was increased from 6 μm to 7 μm (Fig. 7*I*), in agreement with the model prediction.

Discussions

Previous studies proposed that in the absence of cell-matrix adhesion, cells can migrate when confined between two glass coverslips or in a thin micro-fluidic channel by chimneying (17). During chimneying, the cell is hypothesized to exert forces perpendicularly to the confining surfaces as the cell squeeze itself forward. This mechanism is supported by the observations of Malawista *et al*. (22), where leukocytes with β2-integrin adhesion deficiency were seen to migrate in confined environments in between two glass coverslips. However, there have been no reports of how chimneying actually works in amoeboid-like cells. In this study, we have shown how a balance of normal and shear stresses to opposing surfaces generate traction forces necessary for cell migration in the absence of fibronectin-dependent cell-matrix adhesions.

Based on the 3D traction stress measurements, the dHL60 cells that migrated via the amoeboid chimneying mechanism were found to exert mainly normal stresses (along the *z* axis), possibly originating from the cell's intracellular pressure, acting into the gel to anchor themselves between the two gels (Fig. 8, F_{anchor}). The ameoboid cells were also found to exert shearing stresses at the cell front and rear due to bleb protrusion and friction due to cell migration respectively (Fig. 8, $F_{protrusion}$ and $F_{friction}$). We classified the forward motion of dHL60 cells confined between Pluronic-coated gels into three stages. The first stage requires the cell to form at least a bleb at the cell front as the cell body anchored the cell between the two gels. In the second stage, as the bleb grows in size and comes into contact with the gels, the cell migrates into the region where the bleb used to be located and exerts normal anchoring stresses in this region. This allowed the cell to anchor at new positions where the bleb was previously located. In the last stage, the cell body exerts shearing stresses parallel to the gel surface opposite to the direction of migration, which provides friction as the cell squeezes itself forward and the cell rear contracts. These observations are, to the best of our knowledge, the first detailed description of how an amoeboid cell migrate in confined environments via chimneying.

In addition, we found that the anchoring stresses exerted by the cells decrease with increasing gap size as the cell lose contact with the surface of the confining gels. We also note that amoeboid chimneying can only occur if the dHL60 cells are in confined spaces such as in a 3D matrix. Cells do not migrate in the amoeboid mode on unconfined 2D substrates in the absence of cell-matrix adhesion, as they cannot anchor unto a surface to exert forces necessary for migration, even though they continue to form blebs (Fig. 8, Movie S5). Although the extending bleb protrusion would displace the cell's centre of mass forward, subsequent bleb retraction would do the opposite thereby leading to zero net displacement. However, in the presence of cell-matrix adhesions, the dHL60 cells can migrate on

Integrative Biology Accepted Manuscript

unconfined 2D substrates via the mesenchymal mode, by adhering to the substrate and forming lamellipodia.

We also report that the expansive divergent stresses exerted by amoeboid chimneying cells are distinct from the contractile "push-pull" dynamics exhibited by the dHL60 cells that migrate mesenchymally, as well as by other adherent mesenchymal cells such as the fibroblasts (44). These expansive stresses observed in amoeboid cell migration resemble a divergent force dipole (pointing away from the cell body) in contrast to the contractile or convergent force dipole (pointing towards the cell body) (52) during mesenchymal cell migration. The differences in the 3D traction stresses not only offers a mechanistic understanding of the migration processes, it could quantitatively differentiate between the mesenchymal and amoeboid modes of cell migration. Currently, cell migration is classified by subjective morphological differences (e.g. cell shape and the presence of constriction rings) (18,19) or the localization of labeled F-actin to distinguish between blebs or lamellipodia (21,36,37), but the latter will be challenging in cell-types that are difficult to transfect. We propose that a dipole summary of 3D traction stress measurements (44,53-57) can provide the advantage of a quantitative classification of amoeboid and mesenchymal cell migration.

We have shown that integrin-mediated cell-matrix adhesions, although crucial in mesenchymal cell migration, are dispensable in amoeboid cell migration. In the absence of cell-matrix adhesion, dHL60 cells can continue to migrate in confined spaces by employing the amoeboid chimneying mechanism. However, when the dHL60 cells are allowed to adhere to the fibronectin-coated gels, we found that most of the cells formed lamellipodia during migration. Similarly, Bergert *et al*. reported that a suspension subline of Walker 256 carcinosarcoma cells transit from producing bleb-like protrusions to lamellipodia-like protrusions upon crossing from a region without cell-substrate adhesion to a region with cell-substrate adhesion and vice versa (62). These findings suggest that transitions between amoeboid and mesenchymal cell migration can be controlled by changes in cell-matrix adhesivity.

Our results also revealed that unlike mesenchymal cell migration which is known to be altered by ECM rigidity (30-34,39-41,58-61), rigidity do not seem to play an important role in determining amoeboid chimneying speed. This is not unexpected as researchers have hypothesized that mesenchymal cells sense the ECM rigidity through proteins related to the focal adhesion complexes (32,59,63). In the absence of integrin-mediated cell-matrix adhesions where focal adhesion complexes are absent, cells migrating in the amoeboid manner will unlikely be able to "feel" the matrix rigidity if the rigidity sensor is related to the focal adhesion complexes.

However, we found that amoeboid chimneying speed showed a biphasic relationship with the amount of confinement experienced by the cells. Our computational model predicts that the critical gap size before non-polarized blebs begin to form, is determined by the membrane-cortex adhesion strength, which is mediated by the ERM proteins (17,50). This prediction was verified experimentally by treating dHL60 cells with the ezrin inhibitor baicalein. We suggest that reducing membrane-cortex adhesion strength can inhibit directed amoeboid cell migration through narrow pores in the 3D ECM. In agreement with our hypothesis, Diz-Munoz *et al*. have demonstrated that when the membrane-cortex adhesion strength mediated by ezrin is weakened in zebrafish mesoderm-endoderm germ-layer progenitor cells, cells produced more blebs and are less directed than wild-type cells (36). We propose that the inhibition of ERM activity may cause more non-polarized blebs to form

Integrative Biology Accepted Manuscript

which hampers the cell's ability to squeeze through narrow pores in the ECM in a directed manner. This could present a potential target for inhibiting cancer cell metastasis where cells utilize the amoeboid mode to migrate. During cancer progression, cells may over-express ERM proteins that strengthen the membrane-cortex adhesion strength and reduce non-polarized bleb formation, thereby allowing cells to migrate efficiently between narrow pores in the 3D ECM. Indeed, reports have shown that over-expression of ezrin is important in the dissemination of two pediatric tumors (rhabdomyosarcoma and osteosarcoma) (64,65). Ezrin has also been found to be significantly over-expressed in pancreatic and breast cancer (64-67). However, research on the ERM proteins with regards to cancer progression thus far, has focused mainly on modulation of cell survival pathways due to ezrin signaling (68). Ezrin's role on cell migration, particularly during cancer metastasis, remains largely unknown.

Conclusions

By optimizing confining conditions that promote maximum speed of amoeboid migration, we have detected and measured expansive forces responsible for traction and protrusion. 3D traction stress measurements revealed that these cells exert normal stresses directed away from the cell body and into the gels, to anchor themselves between the two pieces of gels. These expansive and divergent chimneying stresses are distinct from the contractile and convergent "push-pull" stresses exerted by cells migrating with the mesenchymal mode of migration. In addition, we show that the mesenchymal and amoeboid cell migration modes are regulated by different physical properties of the ECM. While cells that migrate in the mesenchymal manner show the expected biphasic response to changes in ECM adhesiveness and rigidity, the speed of cells migrating in the amoeboid chimneying manner is independent of ECM adhesiveness and rigidity. Instead, the chimneying cells show a biphasic response to changes in the extent of cell confinement. These observations led us to propose that mechanisms leading to amoeboid and mesenchymal cell migration are mutually exclusive and independently regulated by different physical parameters in the ECM. It could be possible that a cell sense the physical properties of its environment and choose the migratory mode most favorable to navigate through the ECM. This reiterates the importance of understanding the detailed mechanisms that cells employ to sense their physical environment. Such knowledge will be crucial in identifying potential drug targets for cancer therapy to prevent cancer cell metastasis. Although more work remains to be done in order to elucidate the detailed mechanisms involved, our study here has revealed that intracellular pressure and membrane-cortex adhesion strength are important factors that determined the efficiency of amoeboid cell migration in confined environments. Whether and how an amoeboid cell alter its membrane-cortex adhesion strength in response to a chemoattractant or mechanical perturbations in the ECM would therefore be an interesting focus for future studies.

Methods & Materials

Cell culture, differentiation and transfection of HL60 cells

Human promyelocytic leukemia (HL60) cells (ATCC,Manassas, VA) were maintained at 37°C and 5% CO_2 in Roswell Park Memorial Institute medium (RPMI, ATCC) supplemented with 10% fetal bovine serum (GIBCO, Grand Island, NY) and 1% penicillin-streptomycin (GIBCO). The HL60 cells were differentiated into neutrophils (dHL60 cells) by culturing cells in culture media containing 1.3% dimethylsulfoxide (DMSO) for 6 days, following

Integrative Biology Accepted Manuscript

published protocols (69-71). Approximately 72% of the 300 cells counted had differentiated into neutrophils as detected by the nitrobluetetrazolium (NBT) reduction test (69,70) (Fig. *S2*). The diameter of the dHL60 cells was estimated by fitting circles to phase contrast images of the suspended dHL60 cells in MATLAB (imfindcircles) (Fig. *S3*). The diameter of the dHL60 cells was found to be 9.21 ± 0.088 μm (mean ± standard error, n = 306).

The dHL60 cells were transfected with Lifeact-GFP by electroporation (Neon Transfection System) at 1350 V, 35 ms, 1 pulse, to visualize F-actin localization within the cells without compromising actin dynamics (37). To investigate the role of myosin contractility during cell migration, the cell migration speeds were measured (refer to section on quantification of cell migration speed below) immediately after treatment with 50 μM (final concentration) blebbistatin (Tocris Bioscience, Bristol, United Kingdom). Ezrin-mediated association of the actin cortex to the cell membrane was disrupted by treating cells with 20 μM (final concentration) baicalein (Sigma-Aldrich, St. Louis, MO) and measuring cell migration speed 24 h later.

Preparation of polyacrylamide gels bonded to glass surfaces

Polyacrylamide gels were prepared at three acrylamide:bisacrylamide ratios (5:0.05, 8:0.1, and 8:0.2 % w/v (Bio-Rad, Hercules, CA) and mixed with a 1/25 volume of 0.2 μm diameter red fluorescent (Ex λ 580 nm, Em λ 605 nm respectively) beads (2% suspension FluoSpheres; Invitrogen, Carlsbad, CA). Polymerization was initiated with 10% ammonium persulfate (Bio-Rad) and catalyzed with N,N,N',N'-Tetramethylethlenediamine (Bio-Rad). 6 μl of the gel solution was placed on the activated glass-bottomed dish or coverslip (see paragraph below), and covered with an unactivated circular coverslip (12 mm diameter). After polymerization, the top coverslip was carefully removed and the gel was rinsed with 50 mM 4-(2-hydroxyethyl)-1-piperazineethanesulfonic acid (HEPES, pH 8.5; Sigma-Aldrich). The fully hydrated gels from a 6 μl drop were approximately 50-60 μm thick. The Young's moduli of the polymerized gels prepared at the three acrylamide:bisacrylamide ratios were measured by atomic force microscopy (refer to the Supplementary Information and Table *S3*) and the obtained values (1.25 ± 0.016 kPa (mean ± standard error), 6.19 ± 0.053 kPa, and 16.6 ± 0.13 kPa) corresponded with previous measurements (39).

Polyacrylamide gels were bonded to activated glass surfaces which were prepared following the method previously described by Pelham and Wang (30). 20 mm-diameter glass inserts in 35 mm-diameter dishes (ibidi GmbH, Planegg, Germany) and 15 mm-diameter circular coverslips were activated with 3-aminopropyltrimethoxysilane (Sigma-Aldrich) for 5 min, washed with distilled water, covered with 0.5% glutaraldehyde (Sigma-Aldrich) in phosphate buffered saline (PBS) for 30 min, washed twice with distilled water, and left to dry.

The polymerized polyacrylamide gels were functionalized with either fibronectin or a hydrophilic and non-ionic surfactant to control cell-substrate adhesion. Fibronectin-coated gels were prepared by modifying the gel surface with a 0.5 mg/ml solution of the crosslinker, sulfo-succinimidyl-6-(4-azido-2-nitrophenyl-amino) hexanoate (sulfo-SANPAH; Pierce, Rockford, IL) in 50 mM HEPES (pH 8.5), followed by exposure to ultra-violet (UV) light in a sterile hood for 15 min. The darkened sulfo-SANPAH solution was removed and gels were rinsed twice with HEPES for 15 min each. The gels were then covered by 100 μg/ml fibronectin (Sigma-Aldrich) in PBS for 2 h at room temperature on a rocker. To compare adhesion and non-adhesion-dependent cell migration, we prepared gels to which cells were

Integrative Biology Accepted Manuscript

unable to attach, by immersing gels in 0.1% Pluronic F127 (BASF, Ludwigshafen, Germany), a hydrophilic and non-ionic surfactant, for 1 h at room temperature on a rocker (Pluronic-coated gels) (72). The gels (both fibronectin- and Pluronic-coated gels) were then rinsed with PBS, sterilized by exposure to UV light in a sterile hood for 15 min, and incubated for 30 min in the cell culture media at 37°C before cells were transferred to the gels.

Assembly of an *in vitro* cell motility assay to study migration in a confined environment

To mimic a confined 3D environment where cells have to migrate through pores in the ECM, the 9.2 μm-diameter dHL60 cells were sandwiched between a top and bottom polyacrylamide gel (Fig. 1*A-B*) separated by a 120 μm thick spacer (Secure-Seal; Invitrogen). Cells were sandwiched between either fibronectin-coated surfaces to study adhesion-dependent motility or Pluronic-coated surfaces to study adhesion-independent motility. The cells were first allowed to settle onto a fibronectin- or Pluronic-coated gel surface for 15 min. To ensure that only adherent cells were studied, the fibronectin-coated gel, which was attached to a coverslip, was inverted over a spacer on a glass-bottomed dish containing another fibronectin-coated bottom gel. In the case where adhesion-independent motility was studied, a second Pluronic-coated gel, attached to a coverslip, was overlaid onto a spacer on the glass bottom dish containing cells on the Pluronic-coated gel. The spacing between the top and bottom gels (gap size) was measured by confocal microscopy of the fluorescent beads embedded within the gel (Fig. *S6*). The gap sizes were determined to be the distance between the first focused plane of the beads on the top and bottom gels and the measured distance was rounded off to the nearest micrometer. Gaps between 0-15 μm were observed due to variations in gel thickness across the sample. However, the range of gap sizes used in these experiments was 2-8 μm. A small weight (3 g) was placed above the top coverslip to minimize drifting of the top gel during image acquisition.

Microscopy

Neutrophil-like migration of dHL60 cells was induced by 100 nM (final concentration) of the chemokine, Formyl-Methionyl-Leucyl-Phenylalanine (FMLP; Sigma-Aldrich) as prior studies have found FMLP to induce polarization and migration of dHL60 cells (42, 73). Indeed, we observed that more dHL60 cells on unconfined fibronectin-coated substrates adhered to the substrates to form lamellipodia when exposed to an uniform concentration of 100nM FMLP (Fig. *S4C-D*, *red boxes*). However, for dHL60 cells on substrates without fibronectin coating (Pluronic-coated), adding FMLP does not induce cells to adhere to the substrate or form lamellipodia (Fig. *S4A-B*). Differential interference contrast (DIC) images of the live cells were obtained every 30 s for 10 min with the Perkin Elmer Ultraview mounted on an Olympus IX-81 microscope with a 60x water objective lens (NA 1.2). Temperature (37°C), humidity (100%) and carbon dioxide concentration (5%) was maintained by enclosure in a plastic box. The cell nuclei were stained with 1 μg/ml Hoechst 34580 (Invitrogen) to enable calculations of the cell migration speed. 3D image stacks of the fluorescent beads embedded within the polyacrylamide gels were also acquired for calculations of the 3D stress imposed by the cells onto the gels.

Integrative Biology Accepted Manuscript

Quantification of cell migration speed, number of blebs and protrusion asymmetry

The cell migration speed was determined from time-lapsed images of the dHL60 cell nuclei recorded every 30 s, over a period of 10 min. Images of the cell nuclei were segmented in MATLAB by applying a threshold value determined by Otsu's method (74). Nuclei which contacted the edges of the image frame were removed and the nuclei centroid positions ($\vec{r}(t)$) were determined. A MATLAB tracking program, which computes the correlation of the nuclei centroid positions between time frames, was then applied to obtain the cell trajectories (75). The total distance travelled by the cell during the time period of 10 min was obtained by summing the displacements of the nuclei centroid between each 30 s time frame. The cell speed was calculated by dividing the total distance travelled by the cells with the time period observed (10 min).

The mean squared displacement (MSD) of the cell was calculated as

$$MSD\left(\Delta t\right) = \left\langle \left[\vec{r}(t+\Delta t) - \vec{r}(t)\right]^2 \right\rangle, \qquad (1)$$

where Δt is the time interval used to calculate the cell displacement, and $\langle\ \rangle$ represents a moving average (39,42). The MSD versus Δt was then plotted as a log-log plot, and the slope of the data (β), which characterizes the persistence of the motion, was measured.

$$MSD(\Delta t) \propto \Delta t^{\beta} \qquad (2)$$

A value of $\beta = 1$ describes random and diffusive motion while the theoretical upper limit of $\beta = 2$ describes ballistic, directed motion at a constant speed.

The number of blebs produced by the dHL60 cells per minute was obtained from the DIC time-lapse images by manual counting of the total number of blebs produced per cell over a period of 10 min. The centroid positions of each bleb were marked manually and the angle between neighboring blebs was defined by the positions of the bleb centroids relative to the nucleus centroids. For each cell, a coefficient of variance (CV) was evaluated as the ratio of the standard deviation of the angles between neighboring blebs to the mean of the angles between neighboring blebs. This CV measures the degree of protrusion asymmetry, with a value of 0 indicating no protrusion asymmetry and a larger value indicating more asymmetric protrusions.

3D traction stress calculations

The 3D traction stresses exerted by the cells on the polyacrylamide gels were calculated with the digital volume correlation (DVC) algorithm first described by Franck *et al*. (44,53,76). Two volumes of the 3D image stacks of the beads' position within the unstrained (where cells were more than 20 μm away) and the strained gels were obtained and divided into sub-volumes Ω. The fluorescence intensity of the beads in each 3D sub-volume of the unstrained and the strained gel was represented by $f(x_1,x_2,x_3)$ and $g(x_1,x_2,x_3)$ respectively, where x_1, x_2, and x_3 correspond to the Cartesian coordinates along the x, y, and z axes.

The displacement vectors $\boldsymbol{u}$ between each corresponding sub-volumes were estimated from the locations where the cross-correlation, $m(\boldsymbol{u})$, value is maximum. The cross-correlation function is defined by:

Integrative Biology Accepted Manuscript

$$m(\boldsymbol{u}) = \int f(\boldsymbol{x}) g(\boldsymbol{x}+\boldsymbol{u}) d\Omega_x \qquad (3)$$

The cross correlation function can be efficiently computed with Fourier transforms as denoted by Eq. (4),

$$m(\boldsymbol{u}) = F^{-1}\left\{F\left[f(\boldsymbol{x})\right]^* F\left[g(\boldsymbol{x})\right]\right\}, \qquad (4)$$

where the Fourier transform of $f(\mathbf{x})$ is defined by $F\left[f(\boldsymbol{x})\right] = \int f(\boldsymbol{x}) e^{-ikx} d\Omega_x$, *denotes the complex conjugate, and F^{-1} denotes the inverse Fourier transform.

The mean displacement at cell-free regions, where the cell was at least 5 μm away, was also subtracted from the calculated displacement vectors to correct for sample drift during image acquisition. The resultant displacement matrix $\boldsymbol{u}$ approximates the local gel deformation for each sub-volume which best fit the strained image to the unstrained image. After obtaining $\boldsymbol{u}$, a displacement-gradient technique was applied to obtain the strain tensor $\boldsymbol{\varepsilon}$ by minimizing the vector $\boldsymbol{S}$ in a least square fashion (53),

$$\boldsymbol{S} = \sum_{i=1}^{3}\sum_{j=1}^{3}\sum_{k=1}^{3}\left(u_{ijk} - \hat{u}_{ijk}\right)^2, \qquad (5)$$

where $u_{ijk}(x_1, x_2, x_3)$ represents the calculated displacement and $\hat{u}_{ijk}(x_1, x_2, x_3)$ represents the theoretical displacement given by $\hat{u}_{ijk}(x_1, x_2, x_3) = ax_1 + bx_2 + cx_3 + d$. The constants a, b, c, and d were determined by the least square minimization of Eq. (5) with a 3×3×3 pixel kernel. The strain tensor $\boldsymbol{\varepsilon}$ was obtained from the constants a, b, c, and d and can be written in a matrix form:

$$\boldsymbol{\varepsilon} = \begin{pmatrix} \varepsilon_{11} & \varepsilon_{12} & \varepsilon_{13} \\ \varepsilon_{21} & \varepsilon_{22} & \varepsilon_{23} \\ \varepsilon_{31} & \varepsilon_{32} & \varepsilon_{33} \end{pmatrix} = \begin{pmatrix} a & \frac{1}{2}(a+b) & \frac{1}{2}(a+c) \\ \frac{1}{2}(a+b) & b & \frac{1}{2}(b+c) \\ \frac{1}{2}(a+c) & \frac{1}{2}(b+c) & c \end{pmatrix}. \qquad (6)$$

Assuming that the material is linearly elastic, isotropic and incompressible, the material stress tensor $\boldsymbol{\sigma}$ was then determined from the materials constitutive relation:

$$\boldsymbol{\sigma} = E\boldsymbol{\varepsilon} / (1+\nu), \qquad (7)$$

where E is the Young's modulus of the gel and ν is the Poisson's ratio of the gel ($\nu = 0.5$).

The traction stress vector $\boldsymbol{F}$ was calculated at the surface of the gel from the Cauchy relationship,

$$\boldsymbol{F} = \boldsymbol{\sigma} \cdot \boldsymbol{n}, \qquad (8)$$

where $\boldsymbol{n}$ is the surface normal vector (44).

The stresses exerted by the cells were quantified by $F_{z,net}$ which represents the magnitude of the net vector sum of stresses in the z-direction ($\vec{F}_z$), at the first z-plane of the gel immediately next to the cells ($k = 0.25\mu m$).

Integrative Biology Accepted Manuscript

$$F_{z,net} = \left| \sum_{i=1}^{m} \sum_{j=1}^{n} \vec{F}_z(i,j,0.25) \right| \qquad (9)$$

where m and n denotes the number of sub-volumes in the x and y directions respectively.

We also calculated the average stress magnitude over the cell area $\langle F_{x,y,z} \rangle$, at the first z-plane denoted by k=1 (Eq. (10)).

$$\left\langle F_{x,y,z} \right\rangle = \frac{\sum_{i=1}^{m} \sum_{j=1}^{n} \sqrt{\left|\vec{F}_x(i,j,k)\right|^2 + \left|\vec{F}_y(i,j,k)\right|^2 + \left|\vec{F}_z(i,j,k)\right|^2}}{mn} \qquad (10)$$

Modeling of amoeboid cell migration in confined environments

Details of the computational model have been described elsewhere (47) and elaborated in the Supplementary Information. The physical and numerical parameters of the model is listed in Table S1 and S2 respectively. A schematic diagram of the model is also shown in Fig. *S5*

Briefly, a 2D cell was represented by an elastic actin cortex connected to an elastic cell membrane, through elastic membrane-cortex adhesion proteins. The cell cytoplasm and extracellular fluid were modeled as incompressible and viscous fluids with the same viscosity. At any instance of time, the velocity and the pressure field of the cytoplasmic fluid is described by the Stokes equation (Eq. S1) with no-slip boundary condition imposed on the fluid in contact with the walls, and the equation of continuity (Eq. S2).

The site of bleb formation was initiated by a disruption of 15 out of the 200 membrane-cortex adhesive bonds, at one end of the cell in the middle of the channel. Even though the initial site of bleb nucleation was pre-assigned, the growth of the bleb was spontaneously driven by cytoplasmic pressure. The disruption of the membrane-cortex adhesive bonds reduced local pressure and caused the cytoplasmic fluid to flow down a pressure gradient into the region. Bleb growth was supported by the bending and stretching of the detached cell membrane, and further delamination of the cell membrane from the cortex when the length of the springs representing membrane-cortex adhesion bonds exceeded a critical length l_c. The cell cortex was allowed to reform underneath the cell membrane when a bleb was formed. Imaginary diffusive cortical elements were introduced when a region of the membrane was detached from the cortex. These elements represent the actin monomers which reform the cortex underneath the bleb membrane during bleb retraction and would move towards the bleb membrane with a speed V_c. Once the elements reached a distance D_{equil} from the membrane, the membrane-cortex adhesive springs that were previously broken were reattached and integrated into the cortex of the main cell body. The tension in the cell cortex then drove the bleb to retract as the cell returns to its original shape before bleb formation.

During the process of bleb formation and retraction, net displacement of the cell can be achieved because the shape change of the cell during bleb formation is different from that during bleb retraction. The difference in the cell shape change allowed the cell to propel itself forward in the absence of adhesion to the gel surfaces. The resultant cell speed was obtained by dividing the net displacement of the cell's centre of mass with the time taken. The time

Integrative Biology Accepted Manuscript

taken is fixed at 2.5 min for all simulations as it is the typical time taken for a bleb to grow and retract completely.

The cell's intracellular pressure was defined as the cytoplasmic fluid pressure prior to any blebbing events.

Statistical analysis

Statistical analyses of the data were performed using the 2-tailed Student's t test. $p < 0.05$ (*), $p < 0.01$ (**), or $p < 0.001$ (***) were considered significant.

Immunoblot analysis

Cells were washed in ice-cold PBS twice before being solubilized with ice cold RIPA buffer (Pierce) for 30 min. Lysates were centrifuged at 14,000 × *g* for 15 min at 4°C to pellet the cell debris. The supernatants were then mixed with 2x Laemmli sample buffer (Bio-Rad) and heated at 95 °C for 5 min. The samples are then loaded on 10% sodium dodecyl sulfate polyacrylamide gel, separated via electrophoresis and transferred onto a polyvinylidene difluoride (PVDF) membrane. The blot was then incubated at room temperature for 1 h with 5% bovine serum albumin in Tris-buffered saline with 0.1% Tween (TBST) to block non-specific binding. Subsequently, the blot was incubated with antibodies specific for ezrin (Santa Cruz, Dallas, Texas) and β-actin (Santa Cruz), which were diluted with 5% bovine serum albumin in TBST, for 1 h at room temperature. β-actin was used as a protein loading control. The blot was washed 3 times in TBST, for 5 min each, before and after incubating with a HRP-conjugated secondary antibody (Santa Cruz). The signal was then developed with Amersham ECL Prime Western Blotting Detection Reagent (GE Healthcare Life Sciences, Uppsala, Sweden) and imaged with the ChemiDoc MP imaging system (Bio-Rad).

Acknowledgements

We thank Fong Yin Lim and Yen Ling Koon for help with the computational model, Huiling Chen for help with the 3D traction force calculations, and insightful discussions with Chwee Teck Lim.

References

1. R. Keller, *Curr. Opin. Cell Biol.*, 2005, 17, 533-541.
2. R. Keller, *Science*, 2002, 298, 1950-1954.
3. D. C. Weiser, U. J. Pyati and D. Kimelman, *Genes and Dev.*, 2007, 21, 1559-1571.
4. T. J. Shaw and P. Martin. *J. Cell Sci.*, 2009, 122, 3209-3213.
5. A. J. Singer and R. A. F. Clark, *N. Engl. J. Med.*, 1999, 341, 738-746.
6. P. Friedl and B. Weigelin, *Nature Immunol*., 2008, 9, 960-969.
7. A. O. Anderson and N. D. Anderson, *Immunology*, 1976, 31, 731-748.
8. P. Friedl and D. Gilmour, *Nat. Rev. Mol. Cell Bio.*,2009, 10, 445-457.
9. P. Friedl and K. Wolf, *Nat. Rev. Cancer*, 2003, 3, 362-374.
10. K. W. Jeon (editor), in *The Biology of Amoeba*. Academic Press. 1973.

Integrative Biology Accepted Manuscript

11. R. D. Allen and N. S. Allen, *Annu. Rev. Biophys&Bioeng*,1978, 7, 469-495.
12. P. Bruyn, *Q. Rev. Biol.*, 1947, 22, 1-24.
13. S. O. Mast, *J. Morphol. Physiol.*, 1926,41, 347-425.
14. D. L. Taylor, M. Fechheimer and D. M. Shotton, *Philos. Trans. R. Soc. Lond. B. Biol. Sci.*, 1982, 299, 185-197.
15. E. Evans, *Biophys. J.*, 1993, 64, 1306-1322.
16. G. M. Odell and H. L. Frisch, *J. Theor. Biol*., 1975, 50, 59-86.
17. G. Charras and E. Paluch, *Nat. Rev. Mol. Cell Biol.*, 2008, 9, 730-736.
18. K. Wolf, I. Mazo, H. Leung, K. Engelke, U. H. von Andrian, E. I. Deryugina, A. Y. Strongin, E. B. Bröcker and P. Friedl, *J. Cell Biol.*,2003, 160, 267-277.
19. T. Lammermann, B. L. Bader, S. J. Monkley, T. Worbs, R. Wedlich-Soldner, K. Hirsch, M. Keller, R. Forster, D. R. Critchley, R. Fassler and M. Sixt, *Nature.*, 2008, 453, 51-55.
20. E. Sahai and C. J.Marshall. *Nat. Cell Biol*., 2003, 5, 711-719.
21. H. Blaser, M. Reichman-Fried, I. Castanon, K. Dumstrei, F. L. Marlow, K. Kawakami, L. Solnica-Krezel, C. Heisenberg and E. Raz, *Dev. Cell*,2006, 11, 613-627.
22. S. E. Malawista, A. B. Chevance and L. A. Boxer, *Cell Motil. Cytoskel.*,2000, 46, 183-189.
23. G. Giannone, B. J. Dubin-Thaler, O. Rossier, Y. Cai, O. Chaga, G. Jiang, W. Beaver, H. G. Dobereiner, Y. Freund, G. Borisy and M. P. Sheetz, *Cell*, 2007, 128, 561-575.
24. M. Abercrombie and J. E. Heaysman. *Exp. Cell. Res*., 1953, 5, 111-131.
25. M. Abercrombie, J. E. Heaysman and S. M. Pegrum, *Exp. Cell Res*., 1970, 59, 393-398.
26. S. Munevar, Y.L. Wang and M. Dembo. *Mol. Biol. Cell*, 2001, 12, 3947-3954.
27. P. K. Mattila and P. Lappalainen, Nat. Rev. Mol. Cell Biol.,2008, 9, 446-454.
28. T. D. Pollard and G. G. Borisy, *Cell*, 2003, 112, 453-465.
29. T. Lai and K.-H. Chiam, *Phys. Rev. E.*, 2011,84, 061907.
30. R. J. Pelham and Y. L. Wang. *Proc. Natl. Acad. Sci. USA*, 1997, 94, 13661-13665.
31. M. Dembo and Y-L. Wang. *Biophys J.*, 1999, 76, 2307–2316.
32. C. M. Lo, H. B. Wang, M. Dembo and Y-L. Wang. *Biophys. J.*,2000, 79, 144-152.
33. A. K. Yip, K. Iwasaki, C. Ursekar, H. Machiyama, M.Saxena, H. Chen, I. Harada, K.-H. Chiam and Y. Sawada, *Biophys. J.*, 2013, 104, 19-29.
34. J. P. Califano and C. A. Reinhart-King, *Cell. Mol. Bioeng.*, 2010, 3, 68-75.
35. H. Kress, J. Park, C. O. Mejean, J. D. Forster, J. Park, S. S. Walse, Y. Zhang, D. Wu, O. D. Weiner, T. M. Fahmy and E. R. Dufresne. *Nat Methods*, 2009, 6, 905.
36. A. Diz-Munoz, M. Krieg, M. Bergert, I. Ibarlucea-Benitez, D. J. Muller, E. Paluch and C. P. Heisenberg. *PLoS Biol.*, 2010, 8, e1000544.
37. J. Riedl, A. H. Crevenn, K. Kessenbrock, J. H. Yu, D. Neukirchen, M. Bista, F. Bradke, D. Jenne, T. A. Holak, Z. Werb, M. Sixt and R. Wedlich-Soldner, *Nat. Methods.*,2008, 5, 605- 607.
38. M. Le Berre, J. Aubertin and M. Piel, *Integr. Biol.*, 2012, 4, 1406-1414.
39. K. M. Stroka and H. Aranda-Espinoza, *Cell Motil. Cytoskel.*,2009, 66, 328-341.
40. M. H. Zaman, L. M. Trapani, A. L. Sieminski, D. MacKellar, H. Gong, R. D. Kamm, A. Wells, D. A. Lauffenburger and P. Matsudaira, *Proc. Natl. Acad. Sci. USA*, 2006, 103, 10889-10894.
41. S. R. Peyton and A. J. Putnam, *J. Cell. Physiol.*,2005, 204, 198-209.
42. P. W. Oakes, D. C. Patel, N. A. Morin, D. P. Zitterbart, B. Fabry, J. S. Reichner and J. X. Tang, *Blood*, 2009, 114, 1387-1395.
43. M. P. Stewart, J. Helenius, Y. Toyoda, S. P. Ramanathan, D. J. Muller and A. A. Hyman, *Nature*, 2011, 469, 226-230.
44. S. A. Maskarinec, C. Franck, D. A. Tirell and G. Ravichandran, *Proc. Natl. Acad. Sci. USA*, 2009, 106, 22108- 22113.

Integrative Biology Accepted Manuscript

45. K. A. Beningo, K. Hamao, M. Dembo, Y. Wang and H. Hosoya, *Arch. Biochem. Biophys.*,2006, 456, 224-231.
46. J. Jacobelli, F. C. Bennett, P. Pandurangi, A. J. Tooley and M. F. Krummel,*J. Immunol*., 2009, 182, 2041-2050.
47. F. Y. Lim, Y. L. Koon. and K.-H. Chiam, *Comput. Method Biomec.*, 2013, 1-12.
48. F. Y. Lim, K.-H. Chiam and L. Mahadevan, *Europhys. Lett.*,2012, 100, 28004.
49. A. Lorentzen, J. Bamber, A. Sadok, I. Elson-Schwab and C. J. Marshall, *J. Cell Sci.*, 2010, 124, 1256-1267.
50. G. T. Charras, M. Coughlin, T. J. Mitchison and L. Mahadevan, *Biophys. J.*, 2008, 94, 1836-1853.
51. B. Wu, J. Li, D. Huang, W. Wang, Y. Chen, Y. Liao, X. Tang, H. Xie and F. Tang, *BMC Cancer*, 2011,11, 527.
52. U. S. Schwarz and S. A. Safran, *Rev. Mod. Phys.*, 2013, 85, 1327-1381.
53. C. Franck, S. A. Maskarinec, D. A. Tirrell and G. Ravichandran, *PLoS One*, 2011, 6, e17833.
54. T. M. Koch, S. Munster, N. Bonakdar, J. P. Butler and B. Fabry, *PLoS One.*,2012, 7, e33476.
55. S. S. Hur, Y. Zhao, Y.-S. Li, E. Botvinick and S. Chien, *Cell. Mol. Bioeng*,2009, 2, 425-436.
56. W. R. Legant, J. S. Miller, B. L. Blakely, D. M. Cohen, G. M. Genin and C. S. Chen, *Nat. Methods*,2010, 7, 969-973.
57. W. R. Legant, C. K. Choi, J. S. Miller, L. Shao, L. Gao, E. Betzig and C. S. Chen, *Proc. Natl. Acad. Sci. USA*,2013, 110, 881-886.
58. W. H. Guo, M. T. Frey, N. A. Burnham and Y-L. Wang, *Biophys. J.*, 2006, 90, 2213-2220.
59. M. Prager-Khoutorsky, A. Lichtenstein, R. Krishnan, K. Rajendran, A. Mayo, Z. Kam, B. Geiger and A. D. Bershadsky, *Nat. Cell Biol.*,2011, 13, 1457-1466.
60. S. P. Palecek, J. C. Loftus, M. H. Ginsberg, D. A. Lauffenburger and A. F. Horwitz, *Nature*, 1997, 385, 537-540.
61. R. A. Jannat, M. Dembo and D. A. Hammer, *J. Phys. Condens. Matter*, 2010, 22, 194117.
62. M. Bergert, S. D. Chandradoss, R. A. Desai, and E. Paluch. *Proc. Natl. Acad. Sci. USA*, 2012, 109, 14434-14439.
63. B. Geiger, J. P. Spatz and A. D. Bershadsky, *Mol. Cell Biol.*, 2009, 10, 21-33.
64. C. Khanna, J. Khan, P. Nguyen, J. Prehn, J. Caylor, C. Yeung, J. Trepel, P. Meltzer and L. Helman. *Cancer Res.*, 2001, 61, 3750-3759.
65. Y. Yu, J. Khan, C. Khanna, L. Helman, P. S. Meltzer and G. Merlino, *Nat. Med.*, 2004, 10, 175-81.
66. B. E. Elliott, J. A. Meens, S. K. SenGupta, D. Louvard and M. Arpin. *Breast Cancer Res.*, 2005, 7, R365-R373.
67. Y. Meng, Z. Lu, S. Yu, Q. Zhang, Y. Ma and J. Chen. *J. Transl. Med.*,2010, 8, 61.
68. A. Gautreau, P. Poullet, D. Louvard and M. Arpin. *Proc. Natl. Acad. Sci. USA.*,1999, 96, 7300-7305.
69. C. W. Wei, C. C. A. Hu, C. H. A. Tang, M. C. Lee and J. J. Wang, *FEBS Lett.*, 2002, 531, 421-426.
70. S. J. Martin, J. G. Bradley and T. G. Cotter. *Clin. Exp. Immunol.*, 1990, 79, 448-453.
71. F. Gieseler, P. Meyer, D. Schiffmann and K. Wilms. *Blut*, 1989, 58, 159-163.
72. J. L. Tan, J. Tien, D. M. Pirone, D. S. Gray, K. Bhadriraju and C. S. Chen. *Proc. Natl. Acad. Sci. USA*, 2002, 100, 1484-1489.
73. K. Wong, O. Pertz, K. Hahn and H. Bourne. *Proc. Natl. Acad. Sci. USA*, 2006, 103, 3639-3644.

Integrative Biology Accepted Manuscript

74. N. Otsu, *IEEE T. Syst. Man Cyb*., 1979, 9, 62-66.
75. J. C. Crocker and E. R. Weeks. Particle tracking using IDL, Online, http://www.physics.emory.edu/~weeks/idl/, (accessed March 2008).
76. C. Franck, S. Hong, S. A. Maskarinec, D. A. Tirell and G. Ravichandran. *Exp. Mech.*, 2007, 47, 427-438.

Integrative Biology Accepted Manuscript

Figure legends.

FIGURE 1 Schematics of the mechanisms involved in (A) mesenchymal and (B) amoeboid cell migration.

FIGURE 2 dHL60 cells confined between two pieces of polyacrylamide gels exhibit two different migration modalities: Side (*A*) and top (*B*) view of experimental setup. The cell was confined between the two pieces of gels. Spacers were present to separate the top and bottom coverslips, thereby creating a gap of various sizes between the two gels. Fluorescence beads are embedded within the gels for calculation of traction stresses. (*C*-*G*) DIC images of dHL60 cells: (*C*) Cells on 1.25 kPa fibronectin-coated gel without confinement (*unconfined*, *+Fn*) produced both bleb-like protrusions (*green dashed box*) and lamellipodia (*red box*); Cells showing (*D*-*E*) bleb-like and (*F*-*G*) sheet-like protrusions (*arrows*) when confined between Pluronic- (*confined*, *-Fn*) and fibronectin-coated (*confined*, *+Fn*) gels respectively (Young's modulus of 1.25 kPa with a gap size of 2 μm). (*H*) Percentage of cells which formed blebs (*white*), lamellipodia (*black*) or both (*grey*) when cells are embedded between two pieces of Pluronic- (*-Fn*) and fibronectin-coated (*+Fn*) gels with Young's modulus of 1.25 kPa (*-Fn*: n= 169; *+Fn*: n= 172), 6.19 kPa (*-Fn*: n= 71; *+Fn*: n= 153) and 16.6 kPa (*-Fn*: n= 127; *+Fn*: n= 126). Cells were observed over a period of 10 min. (*I*-*K*) dHL60 cells transfected with Lifeact-GFP and confined between two pieces of 1.25 kPa gels with a gap size of 2 μm. (*I*) A cell which was confined between Pluronic-coated gels, formed bleb-like protrusion (*arrow*) whereby the protrusion was initially devoid of F-actin. (*J*) The actin cortex subsequently reappeared under the protrusion (*arrow*), and another bleb was formed (*arrowhead*). (*K*) A cell which was confined between fibronectin-coated gels, formed lamellipodium (*arrow*) where F-actin is localized at the cell front. Scale bars represent 10 μm.

FIGURE 3 Amoeboid cell migration is independent of gel rigidity and show low persistence: (*A*) Mean speed of migrating dHL60 cells versus gel rigidity on Pluronic- (*-Fn*) and fibronectin- (*+Fn*) coated gels. Cells are confined between gels with gap sizes of 2-8 μm. Error bars represent standard error of the mean. *, **, and *** represents $p < 0.05$, $p < 0.01$, and $p < 0.001$ respectively. n.s. denotes non-significant. (C*onfined -Fn*: n= 254, 64, and 328 for gel rigidity of 1.25, 6.19, and 16.6 kPa respectively; C*onfined +Fn*: n= 289, 98, and 157 for gel rigidity of 1.25, 6.19, and 16.6 kPa respectively; *Unconfined +Fn*, n= 41, 53, and 17 for gel rigidity of 1.25, 6.19, and 16.6 kPa respectively). (*B*-*C*) Representative trajectories of 7 cells confined within (*B*) Pluronic-, and (*C*) fibronectin-coated gels, with rigidity of 16.6 kPa and gap size of 2-8 μm. *x*- and *y*-axis are in units of μm. (D) Mean squared displacement (MSD) versus time interval, Δt, for cells confined between Pluronic- (*-Fn, solid circles*) and fibronectin- (*+Fn, open squares*) coated gels with Young's modulus of 16.6 kPa and gap size of 2-8 μm. Linear fits to the data are represented by the solid and dashed lines respectively (*-Fn*: n= 26; *+Fn*: n= 33).

FIGURE 4 3D traction stress measurements reveal cells migrating in the amoeboid mode exert expansive forces on the confining gels in a chimneying manner in contrast to cells migrating in the mesenchymal mode which exert contractile forces on the gels: (*A*) Schematics of a dHL60 cell confined between two Pluronic-coated gels and migrating via the amoeboid mode. A bleb produced at the cell front (*dashed outline*) exerts a shear stress ($\vec{F}_{protrusion}$) on the gel in the direction of the bleb growth. The cell body also pushes into the gel to anchor the cell between the two gels ($\vec{F}_{anchor}$). As the cells migrate forward, the cell exerts another shear stress that is opposite to direction of migration ($\vec{F}_{friction}$). (*B*-*E*) 3D traction stresses exerted on the gel by a chimneying dHL60 cell confined between 1.25 kPa Pluronic-coated gels, with gap size of 2 μm. *xy*-stress maps of the top gel (*B*) and bottom gel (*E*) in the

Integrative Biology Accepted Manuscript

xy-plane immediately above and below the dHL60 cell. Corresponding *xz*-stress maps at the planes denoted by the white dashed lines are shown in (*C* and *D*) respectively. (*F*) Schematics of a dHL60 cell confined between two fibronectin-coated gels and migrating via the mesenchymal mode. The cell adheres to the top gel and exerts contractile shearing stresses at the cell front and rear ($\vec{F}_{protrusion}$ and $\vec{F}_{retraction}$ respectively). (*G-J*) 3D traction stresses exerted on the gel by dHL60 cell, which migrated mesenchymally, when confined between two fibronectin-coated gels, with gap size of 2 μm. *xy*-stress map of the top gel (*G*) and bottom gel (*J*) in the *xy*-plane immediately above and below the cell. Corresponding *xz*-stress map at the plane denoted by the dashed lines are shown in (*H* and *I*). Dashed arrows denote the direction of cell migration. The cell positions are indicated by the white solid lines in *xy*-stress and the *xz*-stress maps. Scale bars represent 5 μm in the *x*, *y* and *z* directions. Insets in (*B* and *G*) are the DIC images of the corresponding cell.

FIGURE 5 Amoeboid cell progressively exerts chimneying forces at where the bleb was originally formed: (*A-I*) Time-lapsed 3D stresses exerted on the gels by a chimneying dHL60 cell confined between 1.25 kPa Pluronic-coated gels, with gap size of 2 μm. *xz*-stress maps of the (*A*) top and (*B*) bottom gel at the plane denoted by white dashed line in (*C*) the DIC image of the cell in *xy*- plane at the first time point (t=0s). *xz*-stress maps of the (*D*) top and (*E*) bottom gel at the plane denoted by white dashed line in (*F*) the DIC image of the cell in *xy*-plane 30s later (t=30s). *xz*-stress maps of the (*G*) top and (*H*) bottom gel at the plane denoted by white dashed line in (*I*) the DIC image of the cell 60s (t=60s) after the first time point. Dashed arrow denote the direction of cell migration. The bleb and cell positions at t=0s are indicated by the white and black dotted lines while the current cell positions are indicated by the black solid lines. Scale bars represent 5 μm in the *x*, *y* and *z* directions. (*J*) The average stress exerted in the region of the bleb (*white dotted lines* in *A-H*) and other parts of the cell body (*black dotted lines* in *A-H*) at t=0s, as time progressed.

FIGURE 6 Chimneying stresses decrease with increasing gap size between the confining gels: (*A*) Magnitude of the vector sum of $\vec{F}_z$ ($F_{z,net}$) exerted by the dHL60 cells on the top gels versus gap size. (*B*) The average stress magnitude, $\langle F_{x,y,z} \rangle$, across the cell area at the top gel surface exerted by dHL60 cells versus gap size. (*Amoeboid*: n= 11, 9, 10 and 11 for gap sizes from 2, 4, 6, and 8 μm respectively; *Mesenchymal*: n= 7, 8, 6 and 7 for gap sizes from 2, 4, 6, and 8 μm respectively.) Error bars represent standard error of the mean. *, **, and *** represents $p < 0.05$, $p < 0.01$, and $p < 0.001$ respectively. n.s. denotes non-significant. (*C-H*) *xz*-stress maps of a plane in the top gel for dHL60 cells which migrate in the amoeboid (*C, E, G*) and mesenchymal (*D, F, H*) mode, with gap sizes of: (*C-D*) 2 μm, (*E-F*) 4 μm, and (*G-H*) 8 μm. The gels have a Young's modulus of 1.25 kPa. Cells migrating in the amoeboid or mesenchymal modes were on Pluronic- or fibronectin-coated gels respectively. Dashed arrows denote direction of migration. Cell and nuclei positions are indicated by the white and black lines respectively. Scale bars represent 5 μm in the *x* and *z* directions.

FIGURE 7 Amoeboid chimneying speed is biphasic with gap size: (*A-B*) Experimental results: (*A*) Mean cell speed versus gap size when dHL60 cells are confined between gels of rigidity 16.6 kPa. *-Fn*: Pluronic-coated gels, *+Fn*: fibronectin-coated gels, *-Blebbistatin*: without blebbistatin treatment, *+Blebbistatin*: with 50 μM (final concentration) blebbistatin treatment. (*-Fn -Blebbistatin*, n= 21, 42, 64, 65, 56, and 58 for gap sizes from 2, 4, 5, 6, 7 and 8 μm respectively; *-Fn +Blebbistatin*, n= 12, 13, 9, 14, 6, and 11 for gap sizes from 2, 4, 5, 6, 7 and 8 μm respectively; *+Fn -Blebbistatin*, n= 11, 43, 14, 50, 11, and 27 for gap sizes from 2, 4, 5, 6, 7 and 8 μm respectively; *+Fn +Blebbistatin*, n= 25, 41, 20, 41, 14, and 33 for gap sizes from 2, 4, 5, 6, 7 and 8 μm respectively.) (*B*) Mean number of blebs formed per min

Integrative Biology Accepted Manuscript

versus gap size (*solid squares*), and mean CV of angles between neighboring blebs versus gap size (*open circles*), for cells on Pluronic-coated gels of rigidity 16.6 kPa (n= 14, 17, 18, 19, 16, and 14 for gap sizes from 2, 4, 5, 6, 7 and 8 μm respectively). (*C*-*H*) Simulation results from the computational amoeboid cell migration model: (*C*) Cell speed versus ratio of the gap size and cell diameter (*G/D*). (*D*) Intracellular pressure versus *G/D* (*solid squares*), and CV of angles between neighboring blebs versus *G/D* (*open circles*). (*E*-*G*) Bleb protrusions corresponding to points marked by *(e)* - *(g)* respectively, in graphs (*C*-*D*). As the gap size decreases, bigger blebs are formed until intracellular pressure reaches a critical value beyond which blebs are spontaneously formed at both the cell front and rear. (*H*) Cell speed versus *G/D* for various membrane cortex adhesion strengths in the simulation. As membrane-cortex adhesion strength decreases, the optimum value of G/D where migration speed is the fastest is increased. (*I*) Experimental results: Mean cell speed versus gap without (-*Baicalein*) and with (+*Baicalein*) addition of 20 μM (final concentration) of baicalein on 16.6 kPa Pluronic-coated gel (*solid squares* and *open circles* respectively). (-*Baicalein*, n= 21, 42, 64, 65, 56, and 58 for gap sizes from 2, 4, 5, 6, 7 and 8 μm respectively; +*Baicalein*, n= 23, 23, 17, 21, 30, and 28 for gap sizes from 2, 4, 5, 6, 7 and 8 μm respectively.) *Inset in (I):* Ezrin expression in dHL60, with and without 24 h treatment with 20 μM baicalein, was detected by western blotting, with β-actin serving as loading control. Error bars represent standard error of the mean. *, **, and *** represents $p < 0.05$, $p < 0.01$, and $p < 0.001$ respectively. In panel (*I*), blue asterisks refer to the p value for the difference between the cell speed at 2 μm and 7 μm while black asterisks refer to the p value for the difference between the cell speed with and without baicalein treatment.

FIGURE 8 Phase diagram of cell phenotype as a function of gap size and cell-matrix adhesion. Arrows denote the direction of stresses which the cells impose on the gels. Dashed arrows indicate the directions of cell migration.

Integrative Biology Accepted Manuscript

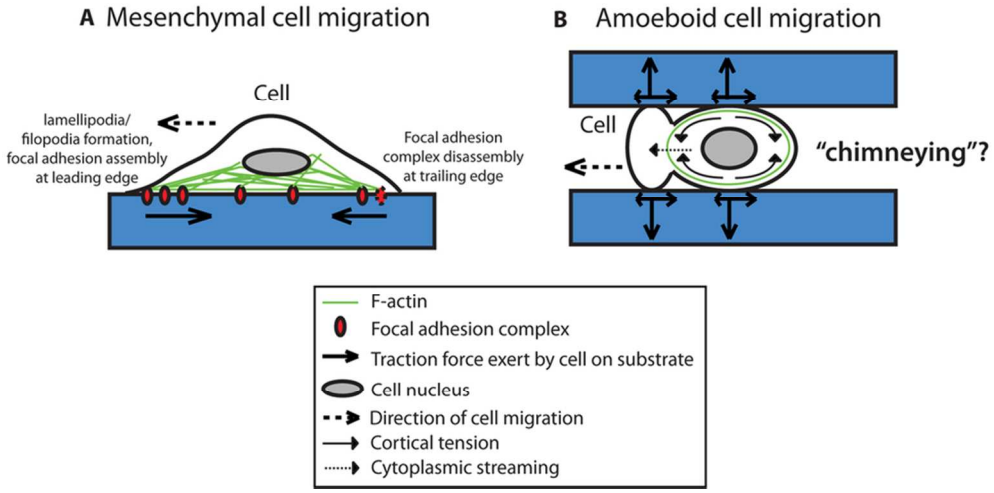

FIGURE 1 Schematics of the mechanisms involved in (A) mesenchymal and (B) amoeboid cell migration.
82x40mm (300 x 300 DPI)

Integrative Biology Accepted Manuscript

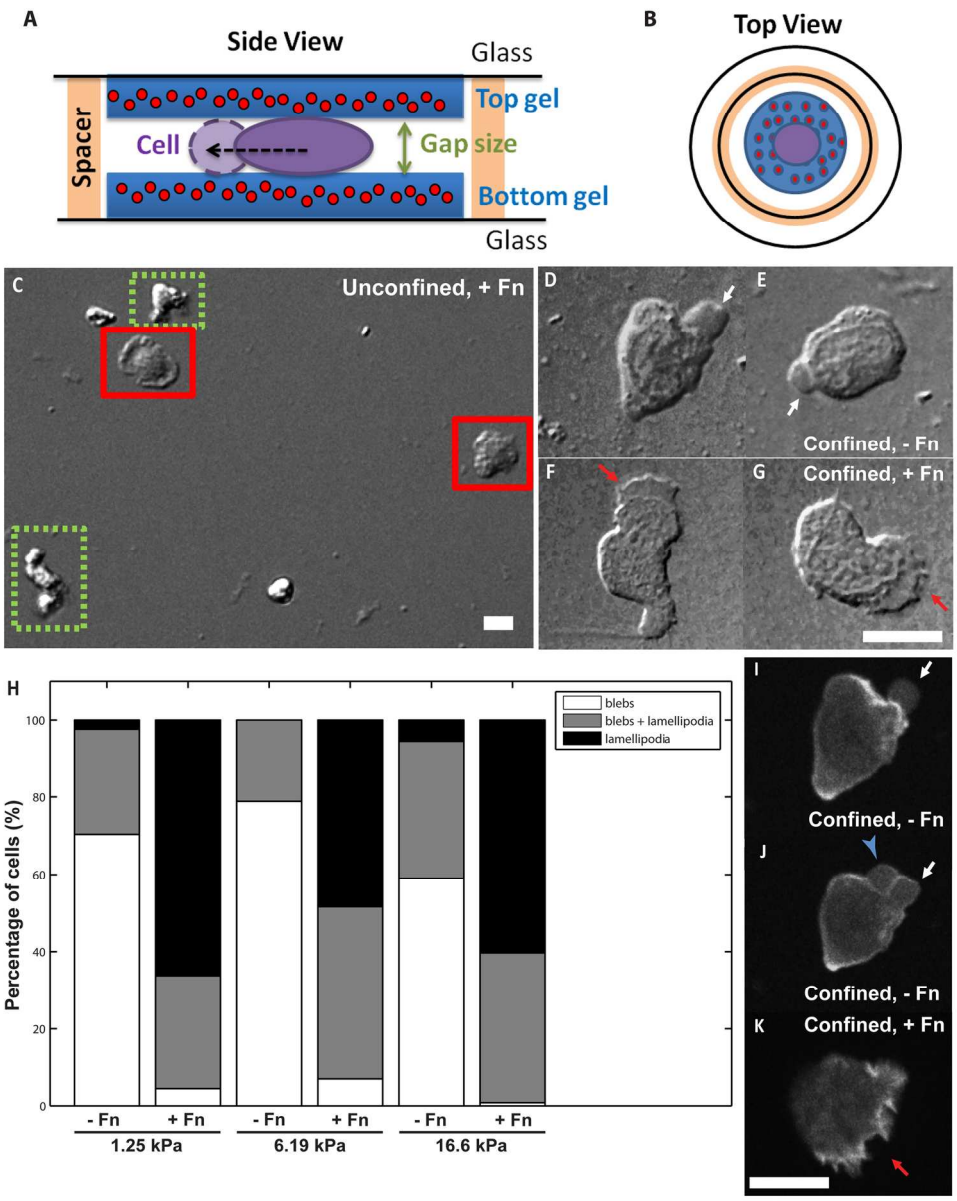

FIGURE 2 dHL60 cells confined between two pieces of polyacrylamide gels exhibit two different migration modalities: Side (A) and top (B) view of experimental setup. The cell was confined between the two pieces of gels. Spacers were present to separate the top and bottom coverslips, thereby creating a gap of various sizes between the two gels. Fluorescence beads are embedded within the gels for calculation of traction stresses. (C-G) DIC images of dHL60 cells: (C) Cells on 1.25 kPa fibronectin-coated gel without confinement (unconfined, +Fn) produced both bleb-like protrusions (green dashed box) and lamellipodia (red box); Cells showing (D-E) bleb-like and (F-G) sheet-like protrusions (arrows) when confined between Pluronic- (confined, -Fn) and fibronectin-coated (confined, +Fn) gels respectively (Young's modulus of 1.25 kPa with a gap size of 2 μm). (H) Percentage of cells which formed blebs (white), lamellipodia (black) or both (grey) when cells are embedded between two pieces of Pluronic- (-Fn) and fibronectin-coated (+Fn) gels with Young's modulus of 1.25 kPa (-Fn: n= 169; +Fn: n= 172), 6.19 kPa (-Fn: n= 71; +Fn: n= 153) and 16.6 kPa (-Fn: n= 127; +Fn: n= 126). Cells were observed over a period of 10 min. (I-K) dHL60 cells transfected with Lifeact-GFP and confined between two pieces of 1.25 kPa gels with a gap size of 2 μm. (I) A cell which

Integrative Biology Accepted Manuscript

was confined between Pluronic-coated gels, formed bleb-like protrusion (arrow) whereby the protrusion was initially devoid of F-actin. (J) The actin cortex subsequently reappeared under the protrusion (arrow), and another bleb was formed (arrowhead). (K) A cell which was confined between fibronectin-coated gels, formed lamellipodium (arrow) where F-actin is localized at the cell front. Scale bars represent 10 μm.
209x256mm (300 x 300 DPI)

Integrative Biology Accepted Manuscript

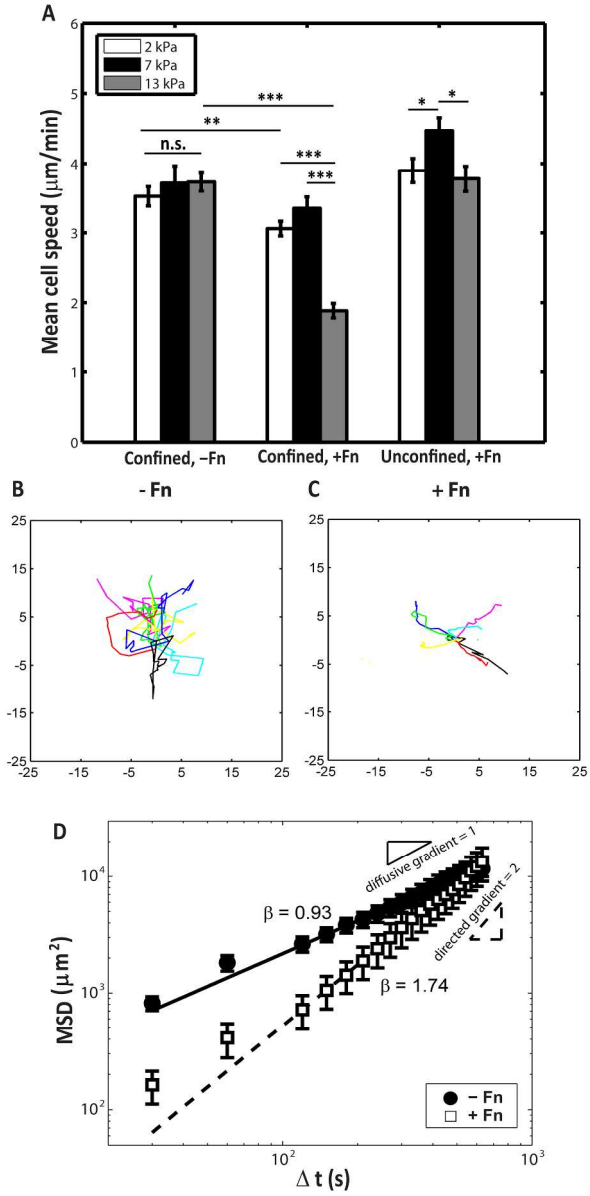

FIGURE 3 Amoeboid cell migration is independent of gel rigidity and show low persistence: (A) Mean speed of migrating dHL60 cells versus gel rigidity on Pluronic- (-Fn) and fibronectin- (+Fn) coated gels. Cells are confined between gels with gap sizes of 2-8 μm. Error bars represent standard error of the mean. *, **, and *** represents $p < 0.05$, $p < 0.01$, and $p < 0.001$ respectively. n.s. denotes non-significant. (Confined -Fn: n= 254, 64, and 328 for gel rigidity of 1.25, 6.19, and 16.6 kPa respectively; Confined +Fn: n= 289, 98, and 157 for gel rigidity of 1.25, 6.19, and 16.6 kPa respectively; Unconfined +Fn, n= 41, 53, and 17 for gel rigidity of 1.25, 6.19, and 16.6 kPa respectively). (B-C) Representative trajectories of 7 cells confined within (B) Pluronic-, and (C) fibronectin-coated gels, with rigidity of 16.6 kPa and gap size of 2-8 μm. x- and y-axis are in units of μm. (D) Mean squared displacement (MSD) versus time interval, Δt, for cells confined between Pluronic- (-Fn, solid circles) and fibronectin- (+Fn, open squares) coated gels with Young's modulus of 16.6 kPa and gap size of 2-8 μm. Linear fits to the data are represented by the solid and dashed lines respectively (-Fn: n= 26; +Fn: n= 33).
343x688mm (300 x 300 DPI)

Integrative Biology Accepted Manuscript

Integrative Biology Accepted Manuscript

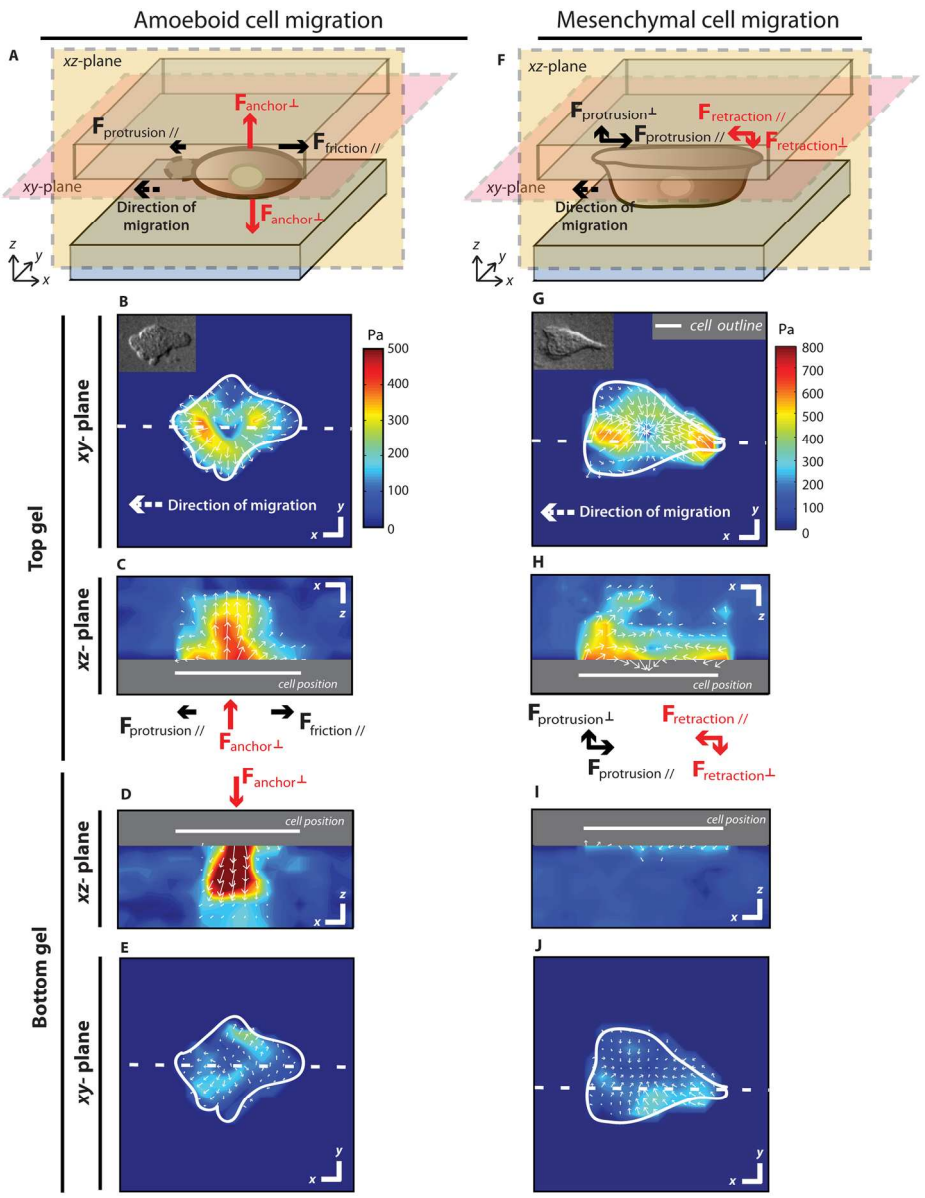

FIGURE 4 3D traction stress measurements reveal cells migrating in the amoeboid mode exert expansive forces on the confining gels in a chimneying manner in contrast to cells migrating in the mesenchymal mode which exert contractile forces on the gels: (A) Schematics of a dHL60 cell confined between two Pluronic-coated gels and migrating via the amoeboid mode. A bleb produced at the cell front (dashed outline) exerts a shear stress (protrusion) on the gel in the direction of the bleb growth. The cell body also pushes into the gel to anchor the cell between the two gels (anchor). As the cells migrate forward, the cell exerts another shear stress that is opposite to direction of migration (friction). (B-E) 3D traction stresses exerted on the gel by a chimneying dHL60 cell confined between 1.25 kPa Pluronic-coated gels, with gap size of 2 μm. xy-stress maps of the top gel (B) and bottom gel (E) in the xy-plane immediately above and below the dHL60 cell. Corresponding xz-stress maps at the planes denoted by the white dashed lines are shown in (C and D) respectively. (F) Schematics of a dHL60 cell confined between two fibronectin-coated gels and migrating via the mesenchymal mode. The cell adheres to the top gel and exerts contractile shearing stresses at the cell front and rear (protrusion and retraction respectively). (G-J) 3D traction stresses exerted on the gel by

Integrative Biology Accepted Manuscript

dHL60 cell, which migrated mesenchymally, when confined between two fibronectin-coated gels, with gap size of 2 μm. xy-stress map of the top gel (G) and bottom gel (J) in the xy-plane immediately above and below the cell. Corresponding xz-stress map at the plane denoted by the dashed lines are shown in (H and I). Dashed arrows denote the direction of cell migration. The cell positions are indicated by the white solid lines in xy-stress and the xz-stress maps. Scale bars represent 5 μm in the x, y and z directions. Insets in (B and G) are the DIC images of the corresponding cell.
222x289mm (300 x 300 DPI)

Integrative Biology Accepted Manuscript

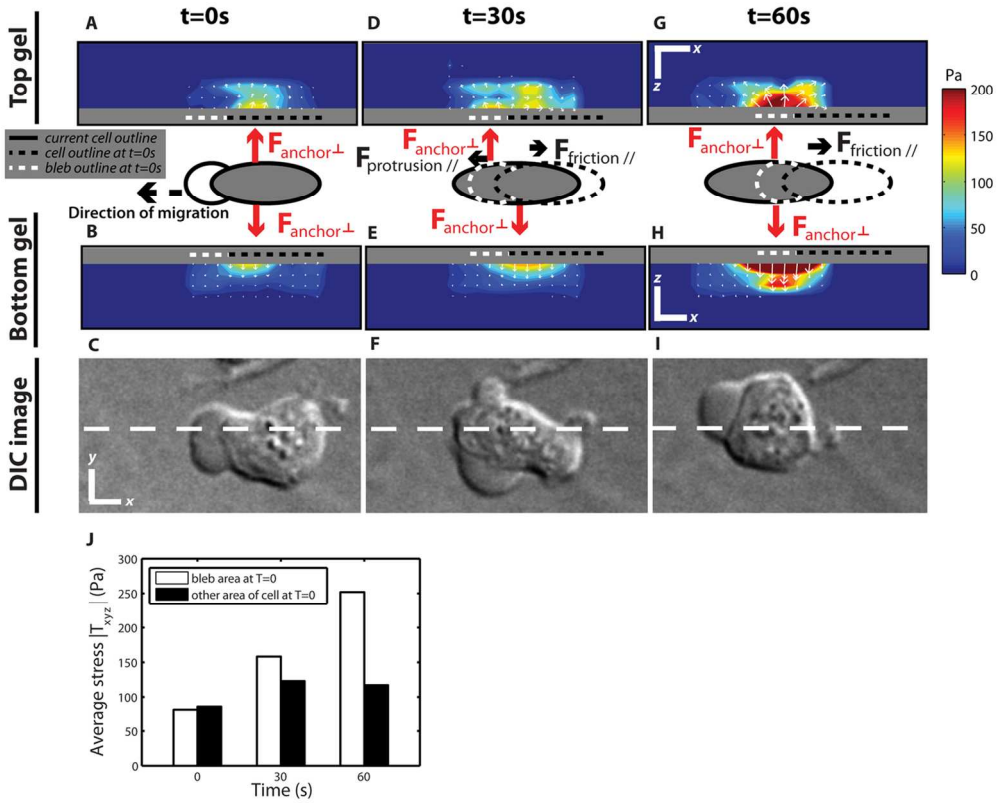

FIGURE 5 Amoeboid cell progressively exerts chimneying forces at where the bleb was originally formed: (A-I) Time-lapsed 3D stresses exerted on the gels by a chimneying dHL60 cell confined between 1.25 kPa Pluronic-coated gels, with gap size of 2 μm. xz-stress maps of the (A) top and (B) bottom gel at the plane denoted by white dashed line in (C) the DIC image of the cell in xy- plane at the first time point (t=0s). xz-stress maps of the (D) top and (E) bottom gel at the plane denoted by white dashed line in (F) the DIC image of the cell in xy- plane 30s later (t=30s). xz-stress maps of the (G) top and (H) bottom gel at the plane denoted by white dashed line in (I) the DIC image of the cell 60s (t=60s) after the first time point. Dashed arrow denote the direction of cell migration. The bleb and cell positions at t=0s are indicated by the white and black dotted lines while the current cell positions are indicated by the black solid lines. Scale bars represent 5 μm in the x, y and z directions. (J) The average stress exerted in the region of the bleb (white dotted lines in A-H) and other parts of the cell body (black dotted lines in A-H) at t=0s, as time progressed.
138x112mm (300 x 300 DPI)

Integrative Biology Accepted Manuscript

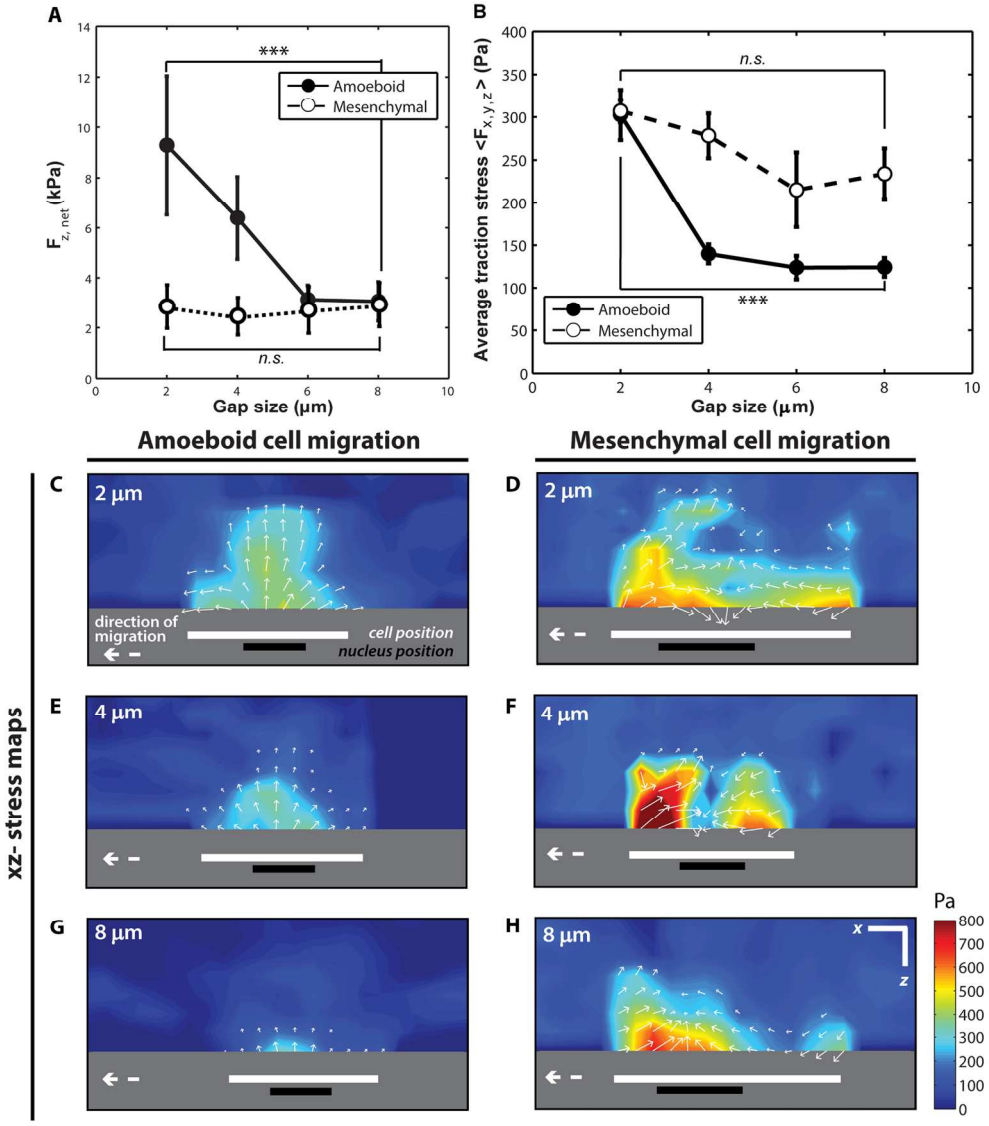

FIGURE 6 Chimneying stresses decrease with increasing gap size between the confining gels: (A) Magnitude of the vector sum of z (Fz,net) exerted by the dHL60 cells on the top gels versus gap size. (B) The average stress magnitude, |Txyz|, across the cell area at the top gel surface exerted by dHL60 cells versus gap size. (Amoeboid: n= 11, 9, 10 and 11 for gap sizes from 2, 4, 6, and 8 μm respectively; Mesenchymal: n= 7, 8, 6 and 7 for gap sizes from 2, 4, 6, and 8 μm respectively.) Error bars represent standard error of the mean. *, **, and *** represents $p < 0.05$, $p < 0.01$, and $p < 0.001$ respectively. n.s. denotes non-significant. (C-H) xz-stress maps of a plane in the top gel for dHL60 cells which migrate in the amoeboid (C, E, G) and mesenchymal (D, F, H) mode, with gap sizes of: (C-D) 2 μm, (E-F) 4 μm, and (G-H) 8 μm. The gels have a Young's modulus of 1.25 kPa. Cells migrating in the amoeboid or mesenchymal modes were on Pluronic- or fibronectin-coated gels respectively. Dashed arrows denote direction of migration. Cell and nuclei positions are indicated by the white and black lines respectively. Scale bars represent 5 μm in the x and z directions.
192x217mm (300 x 300 DPI)

Integrative Biology Accepted Manuscript

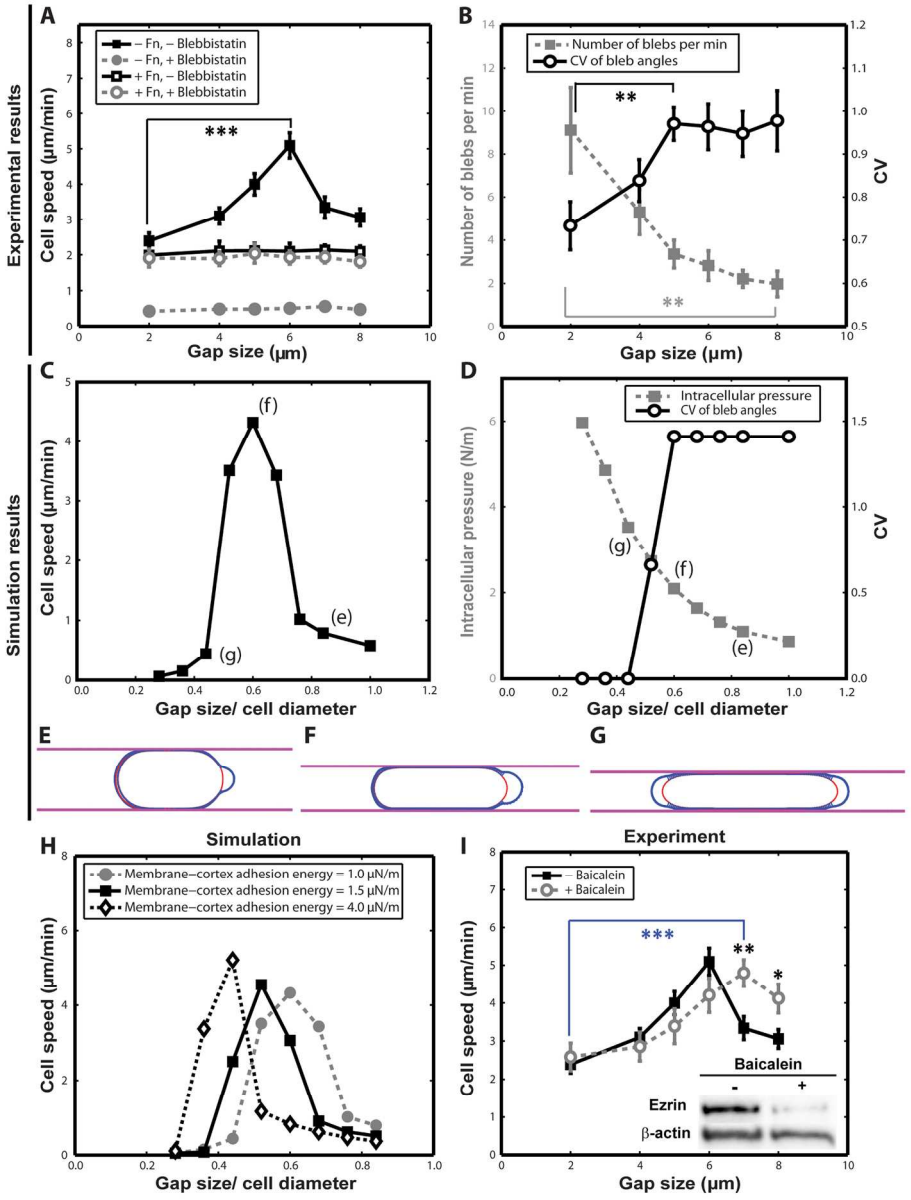

FIGURE 7 Amoeboid chimneying speed is biphasic with gap size: (A-B) Experimental results: (A) Mean cell speed versus gap size when dHL60 cells are confined between gels of rigidity 16.6 kPa. -Fn: Pluronic-coated gels, +Fn: fibronectin-coated gels, -Blebbistatin: without blebbistatin treatment, +Blebbistatin: with 50 μM (final concentration) blebbistatin treatment. (-Fn -Blebbistatin, n= 21, 42, 64, 65, 56, and 58 for gap sizes from 2, 4, 5, 6, 7 and 8 μm respectively; -Fn +Blebbistatin, n= 12, 13, 9, 14, 6, and 11 for gap sizes from 2, 4, 5, 6, 7 and 8 μm respectively; +Fn -Blebbistatin, n= 11, 43, 14, 50, 11, and 27 for gap sizes from 2, 4, 5, 6, 7 and 8 μm respectively; +Fn +Blebbistatin, n= 25, 41, 20, 41, 14, and 33 for gap sizes from 2, 4, 5, 6, 7 and 8 μm respectively.) (B) Mean number of blebs formed per min versus gap size (solid squares), and mean CV of angles between neighboring blebs versus gap size (open circles), for cells on Pluronic-coated gels of rigidity 16.6 kPa (n= 14, 17, 18, 19, 16, and 14 for gap sizes from 2, 4, 5, 6, 7 and 8 μm respectively). (C-H) Simulation results from the computational amoeboid cell migration model: (C) Cell speed versus ratio of the gap size and cell diameter (G/D). (D) Intracellular pressure versus G/D (solid squares), and CV of angles between neighboring blebs versus G/D (open circles). (E-G) Bleb protrusions

Integrative Biology Accepted Manuscript

corresponding to points marked by (e) - (g) respectively, in graphs (C-D). As the gap size decreases, bigger blebs are formed until intracellular pressure reaches a critical value beyond which blebs are spontaneously formed at both the cell front and rear. (H) Cell speed versus G/D for various membrane cortex adhesion strengths in the simulation. As membrane-cortex adhesion strength decreases, the optimum value of G/D where migration speed is the fastest is increased. (I) Experimental results: Mean cell speed versus gap without (-Baicalein) and with (+Baicalein) addition of 20 μM (final concentration) of baicalein on 16.6 kPa Pluronic-coated gel (solid squares and open circles respectively). (-Baicalein, n= 21, 42, 64, 65, 56, and 58 for gap sizes from 2, 4, 5, 6, 7 and 8 μm respectively; +Baicalein, n= 23, 23, 17, 21, 30, and 28 for gap sizes from 2, 4, 5, 6, 7 and 8 μm respectively.) Inset in (I): Ezrin expression in dHL60, with and without 24 h treatment with 20 μM baicalein, was detected by western blotting, with β-actin serving as loading control. Error bars represent standard error of the mean. *, **, and *** represents $p < 0.05$, $p < 0.01$, and $p < 0.001$ respectively. In panel (I), blue asterisks refer to the p value for the difference between the cell speed at 2 μm and 7 μm while black asterisks refer to the p value for the difference between the cell speed with and without baicalein treatment.
224x294mm (300 x 300 DPI)

Integrative Biology Accepted Manuscript

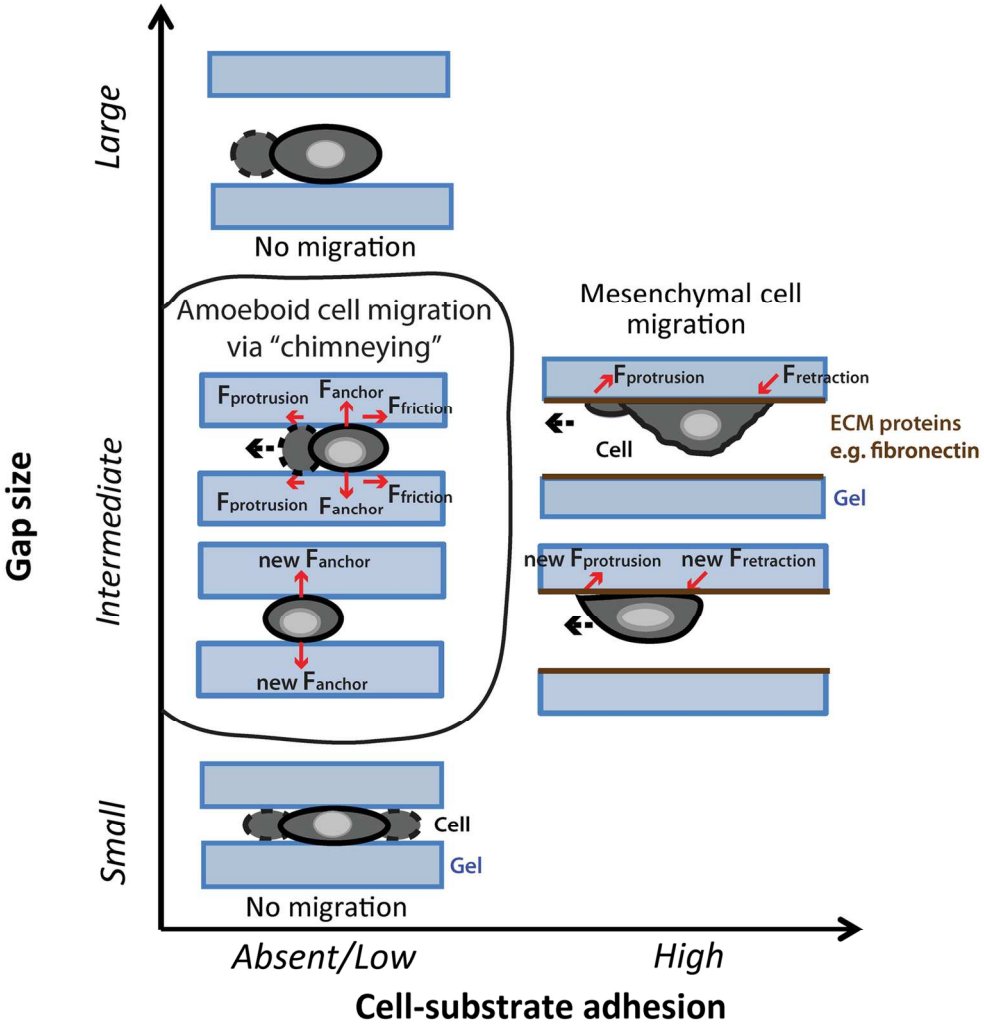

FIGURE 8 Phase diagram of cell phenotype as a function of gap size and cell-matrix adhesion. Arrows denote the direction of stresses which the cells impose on the gels. Dashed arrows indicate the directions of cell migration.
178x187mm (300 x 300 DPI)

Integrative Biology Accepted Manuscript